ACK1 and BRK non-receptor tyrosine kinase deficiencies are associated with familial systemic lupus and involved in efferocytosis

Authors: Stephanie Guillet[1,2#], Tomi Lazarov[1,3#], Natasha Jordan[4], Bertrand Boisson[5,6], Maria Tello[1], Barbara Craddock[7], Ting Zhou[8], Chihiro Nishi[9], Rohan Bareja[10], Hairu Yang[1], Frederic Rieux-Laucat[6], Rosa Irene Fregel Lorenzo[11] Sabrina D. Dyall[12], David Isenberg[13], David D'Cruz[4], Nico Lachmann[14], Olivier Elemento[10], Agnes Viale[15], Nicholas D. Socci[15,16], Laurent Abel[5,6], Shigekazu Nagata[9], Morgan Huse[1], W. Todd Miller[7&], Jean-Laurent Casanova[5,6,17,18,19 &], Frederic Geissmann[1,3,4 $].

Affiliations:

1. Immunology Program, Sloan Kettering Institute, Memorial Sloan Kettering Cancer Center, New York, New York 10065, USA
2. Ecole doctorale Bio Sorbonne Paris Cité, Université Paris Descartes-Sorbonne Paris Cité. Paris, France.
3. Immunology and Microbial Pathogenesis Program, Weill Cornell Graduate School of Medical Sciences, New York, New York 10065, USA
4. Centre for Molecular and Cellular Biology of Inflammation (CMCBI), King's College London and Louise Coote Lupus Unit, Guy's and Thomas' Hospitals, London SE1 1UL, UK
5. St. Giles Laboratory of Human Genetics of Infectious Diseases, Rockefeller Branch, The Rockefeller University, New York, 10065 NY, USA
6. University of Paris Cité, Imagine Institute, Paris, France.
7. Department of Physiology and Biophysics, Stony Brook University School of Medicine, Stony Brook, NY, 11794-8661
8. SKI Stem Cell Research Core**,** Memorial Sloan Kettering Cancer Center, New York, New York 10065, USA
9. Laboratory of Biochemistry & Immunology, World Premier International Immunology Frontier Research Center, Osaka University, Suita, Osaka 565-0871
10. Cary and Israel Englander Institute for Precision Medicine, Institute for Computational Biomedicine, Meyer Cancer Center Weill Cornell Medical College, New York, New York 10065, USA
11. University of La Laguna, San Cristóbal de La Laguna, Santa Cruz de Tenerife - Spain (38200)
12. Department of Biosciences and Ocean Studies, Faculty of Science, University of Mauritius, Reduit, Mauritius
13. Centre for Rheumatology, Division of Medicine, University College London, The Rayne Building, University College London.
14. Institute of Experimental Hematology, REBIRTH Cluster of Excellence, Hannover Medical School, Hannover 30625, Germany
15. Marie-Josée & Henry R. Kravis Center for Molecular Oncology, Memorial Sloan Kettering Cancer Center, New York, New York 10065, USA
16. Bioinformatics Core, Memorial Sloan Kettering Cancer Center, New York, New York 10065, USA
17. Howard Hughes Medical Institute, New York, 10065 NY, USA
18. Lab of Human Genetics of Infectious Diseases, INSERM, Necker Hospital for Sick Children, Paris, France, EU
19. Department of Pediatrics, Necker Hospital for Sick Children, Paris, France, EU

[#] SG and TL equally contributed to this study

[&] J-LC and W-TM equally contributed to this study

[$] Correspondence to Frederic Geissmann: geissmaf@mskcc.org

ABSTRACT

Systemic Lupus Erythematosus (SLE) is an autoimmune disease, the pathophysiology and genetic basis of which are incompletely understood. Non-receptor tyrosine kinases (NRTKs) regulate activation, migration, and proliferation of immune cells. We report compound heterozygous deleterious variants in the kinase domains of the non-receptor tyrosine kinases (NRTK) TNK2/ACK1 in one multiplex family and PTK6/BRK in another. Experimental blockade of mouse ACK1 or BRK increases glomerular IgG deposits and circulating autoantibodies in an *in vivo* SLE model. In addition, we found that the patients' ACK and BRK variants impair efferocytosis, the MERTK-mediated anti-inflammatory response to apoptotic cells, in human induced Pluripotent Stem Cells (hiPSC)-derived macrophages. Overall, our data suggest that ACK1 and BRK deficiencies are associated with human SLE and impair efferocytosis.

One sentence summary: Human ACK1 and BRK kinases loss of function variants underlie systemic lupus erythematosus in young patients from multiplex families and disrupt the anti-inflammatory response of macrophages to apoptotic cells.

INTRODUCTION

Systemic lupus erythematosus (SLE) is a chronic autoimmune rheumatic disease, characterized by the presence of circulating autoantibodies against nuclear antigens. Clinical manifestations vary among affected individuals and can involve many organs and systems, including the skin, joints, kidneys, heart, lungs, nervous system, and hematopoietic system [1,2]. The prevalence of SLE ranges from 0.4 to 2 /1,000, and varies with sex, age, and ancestry, being more common in women of childbearing age and individuals of African, Asian, and Hispanic ancestry [1-9]. Sex, hormones, and environmental factors, including drugs and chemical exposures, viral infections, and sunlight, contribute to disease. At present specific therapies for SLE are few and far between [10], and clinical manifestations such as lupus nephritis, one of the most common and serious manifestations of SLE, remain a major risk factor for morbidity and mortality [11-14]. The contribution of genetics to SLE is supported by epidemiological data showing familial aggregation [15-17] and higher concordance rates between monozygotic than dizygotic twins [18], the association of autosomal recessive deficiency in PKCdelta or DNAse1L3 with familial SLE, and similar phenotypes in the corresponding mouse models [19-24]. In addition, genome wide association studies in large populations of patients have implicated a number of genes associated with immune system function [1,25], and an SLE-like disease is observed in a proportion of patients with immunodeficiency due to autosomal recessive or X-linked C1q, C1r/s, C2, C4, and NADPH-Oxidase deficiencies [26-30], with Rasopathies due to autosomal dominant gain-of-function mutations in the RAS pathway [31], and a proportion of patients presenting with interferonopathies with bi-allelic or mono-allelic mutations in genes coding for nucleic acid sensors such as TREX1, STING, SAMHD1, ADAR, and IFIH1 [32-35].

Here, we performed a forward genetic screen in multiplex SLE families with a well-defined phenotype, lupus nephritis, to identify new SLE causing genes and molecular pathways involved in SLE. We report the characterization of novel and rare deleterious variant alleles of two genes encoding the non-receptor tyrosine kinases (NRTK) Tyrosine Kinase Non-Receptor 2 / Activated CDC42 kinase 1 (TNK2/ACK1) and Protein Tyrosine Kinase 6 / Breast Tumor Kinase (PTK6/BRK) in two multiplex families. The variant alleles strongly decrease ACK1 and BRK kinase activity. BRK and ACK1 were shown to control B-cell and T-cell proliferation, survival, and activation [36,37]. Although ACK1- and BRK- genetic deficiency [36-38] or their pharmacological inhibition does not result in spontaneous lupus development in mice, we show that ACK1 or BRK inhibitors aggravate IgG glomerular deposition in the kidneys of BALB/cByJ mice treated with pristane to induce a lupus-like disease [39] and increases serum autoantibody levels. NRTKs mediate phosphorylation of downstream effectors, including RAC1, AKT, and STAT1/3, which are involved in immune cells homeostasis, and their deficiency can cause autoimmunity through different mechanisms [40]. NRTKs such as ACK1 [41], Src [42], and PTK2/FAK [43,44] are also targets of MERTK, which mediates efferocytosis, the recognition of phosphatidylserine (PtdSer) on apoptotic cells for their anti-inflammatory engulfment [45-48]. MERTK deficiency is a cause of SLE-like disease [48]. We found that the patients' ACK1 and BRK variants are kinase dead in response to MERTK activation and fail to phosphorylate AKT and STAT3, and to activate RAC1. Human iPSC-derived macrophages from patients and isogenic variants presented with defective AKT/STAT3 driven anti-inflammatory response and control of TNF and IL1b production in response to apoptotic cells and had a modest decrease in uptake of apoptotic cells, in comparison to familial and isogenic controls. In contrast, ACK and BRK kinase activity are dispensable for the phagocytosis of polystyrene beads, opsonized cells, and microbes. These results altogether suggest that ACK1 and BRK deficiencies

underlie SLE in the two families, and that a defective efferocytic response to apoptotic cells may contribute to the auto-immune phenotype of the patients.

RESULTS

NRTK compound heterozygous missense variants in two multiplex families with SLE.

We recruited 10 multiplex SLE families, each with 2 or 3 individuals diagnosed with biopsy confirmed lupus nephritis, classified according to the SLICC criteria [2] for whom we obtained genomic DNA (blood) in the Louise Coote Lupus Clinic at Guy's and St Thomas' Hospitals, London. We collected peripheral blood from a total of 22 patients and 17 relatives. Thirty five percent (%) of patients were male, and the same proportion were diagnosed before the age of 18 years. Genomic DNA was submitted to whole exome sequencing. Polymorphisms with a minor allele frequency (MAF) >0.01 in the publicly available database gnomAD (120,000 individuals), 1,000 genome Project (2,504 individuals) and our in-house database (>10,000 individuals) were excluded from analysis. We analyzed each kindred independently, under X-linked recessive, autosomal dominant, or autosomal recessive models of inheritance, and this analysis identified candidate genes in two kindreds.

In Family 1, we identified compound heterozygous missense variants in the non-receptor tyrosine kinase (NRTK) ACK1, which were confirmed by Sanger sequencing (**Figure 1A, Figure 1-figure supplement 1**). The 2 patients were males and developed a class IV lupus nephritis between age 10-15 . The K161Q allele was inherited from one parent and A156T from the other (**Figure 1A**). Principal components analysis (PCA) based on the whole-exome sequencing to analyze population structure, parental inbreeding, and familial linkage [49] reveals South Asian ancestry, the closest 1,000 Genomes Project individuals being those from North India (India, Bangladesh, and Pakistan, see Methods). The ACK1 mutant alleles, A156T and K161Q (transcript ENST00000333602, **Figure 1-figure supplement 1**), have not been reported in South Asian (31,442 alleles) or other populations from public database (gnomAD, 1,000 genomes project) or our own in-house databases of >10,000 exomes of patients with infectious phenotypes. Finally, these variants were not found in DNA from 100 individuals from the small south eastern island from which they originated (see Methods). Altogether, ACK1 mutant alleles, A156T and K161Q are private to this family and their segregation is compatible with an autosomal recessive trait with complete penetrance.

In Family 2, we identified compound heterozygous missense variants in another NRTK, BRK in three siblings (**Figure 1B, Figure 1-figure supplement 1**). Two patients developed lupus nephritis, and the third patient developed a severe panniculitis, between the ages of 20 and 30 year-old. Two patients were female and one male. One parent, who was not genotyped, probably transmitted the G321R to their children, and the 2 other parents (who are also siblings) transmitted the G257A allele (only one parent was available for genotyping) (**Figure 1B, Figure 1-figure supplement 2**). An unaffected sibling (2.III.2) carries the G321R allele but not the G257A allele (**Figure 1B, Figure 1-figure supplement 2**). PCA analysis showed that individuals from family 2 have Sub-Saharan African ancestry, with the closest populations of 1,000 genomes project being African Caribbean in Barbados and African Ancestry in Southwest US and Luhya in Webuye in Kenya (see Methods). These 2 BRK mutant alleles, G257A and G321R are reported with a maximum MAF of ~ $8x10^{-5}$ and $5x10^{-3}$ respectively in Sub-Saharan African subpopulations (**Figure 1-figure supplement 1**), predicting a homozygosity frequency of ~ 10^{-8} and 10^{-6}

respectively. These alleles are extremely rare outside Africa in the non-African gnomAD populations. These results are fully consistent under a recessive model with the overall prevalence of SLE (40 to 200 per 100,000 individuals). Genes that may cause SLE with high or low penetrance in accordance with their inheritance mode (**Figure 1-figure supplement 3**) were not candidates in these kindreds.

The patients' ACK1 and BRK variants are kinase null and hypomorphic.

The ACK1 K161Q A156T and BRK G257A and G321R variants are all localized in the evolutionarily conserved kinase domains of the 2 proteins **(Figure 1C)**, within the N-terminal (ATP-binding) lobes of the kinase catalytic domains [50,51] **(Figure 1D)**, and near the positions of other mutations that decrease kinase activity [52,53] **(Figure 1C).** The variants are all predicted to be deleterious based on Combined Annotation Dependent Depletion (CADD) corrected with mutation significance cutoffs (MSC) [54,55] (**Figure 1-figure supplement 1**). To examine the functional effects of the mutations, we first expressed mutant forms of ACK1 and BRK in HEK293T cells. *In vitro* kinase assays indicated that ACK1 A156T and BRK G321R are kinase-dead mutants, and that ACK1 K161Q and BRK G257A are severe hypomorphs with a ~ *20%* residual kinase activity *in vitro* (**Figure 2A**). ACK1 A156T and K161Q and BRK G321R variants also lacked auto-phosphorylation activity (**Figure 2B**), phenocopying the effect of the specific ACK1 and BRK kinase inhibitors Aim100 [56] and Cpd4f [57] respectively (**Figure 2C**), while the BRK G257A allele has a small residual activity (**Figure 2C**). To examine the effects of the mutations in the patient's cells we generated induced pluripotent stem cells (iPSC) from unrelated WT donors, patient 1-III-1 (ACK1 mutant), his heterozygous parent 1-II-3, patient 2-III-3 (BRK mutant) and her heterozygous sibling 2-III-2 **(Figure 2-figure supplement 1A-D**), and differentiated them into iPSC-derived macrophages [58] (**Figure 2D, Figure 2-figure supplement 1E**). hiPSC-derived macrophages from unrelated donors, familial controls, and patients presented with a normal morphology, survival, and phenotype and expressed comparable amount of ACK1 and BRK at the transcript and protein level (**Figure 2D, E, Figure 2-figure supplement 1G**)**,** but *in vitro* kinase assay indicated a loss of ACK1 kinase activity in ACK1$^{K161Q/A156T}$ macrophages in comparison to controls (**Figure 2E**)**.** The peptide substrate specificity of BRK overlaps with those of Src family kinases [59] present in the anti-BRK IPs. We therefore studied BRK kinase activity by IP-WB, which showed reduced BRK Tyr342 phosphorylation in BRK$^{G257A/G321R}$ macrophages in comparison to controls (**Figure 2E**). These data altogether indicate that the patients' ACK1 A156T and BRK G321R variants are kinase-dead alleles and K161Q and BRK G257A are severe hypomorphs.

ACK1 and BRK sequences are highly conserved in human populations, when compared with other species (**Figure 1C**). Apart from the alleles we report here, only 90 and 35 predicted loss of function (LOF) alleles are reported in gnomAD for ACK1 or BRK respectively, with MAFs ≤ 10^{-4}, and none of them reported in homozygosity. Conversely, we examined the *in vitro* kinase activity of ACK1 mutants with a MAF≥0.005 and reported as homozygous in gnomAD (n=4). *In vitro* kinase activity of these variants was normal (**Figure 2-figure supplement 2**). There was no BRK mutant with MAF≥0.005 reported as homozygous in gnomAD. Thus, autosomal recessive deficiency for either protein, whether complete or partial, is expected to be well below 1/100,000 in the general population, which is compatible with autosomal recessive ACK1 and BRK deficiencies underlying SLE in patients from these two kindreds.

ACK1 and BRK inhibition exacerbates pristane-induced SLE in Balb/c mice.

ACK1- and BRK-deficient T cells are characterized by increased proliferation and activation [36,37]. However, ACK1- and BRK-deficient mice do not develop Lupus-like disease on a C57BL/6 background [36-38], and weekly injection of either Aim100 [56] or Cpd4f [57] for 12 weeks in susceptible wild-type (WT) BALB/cByJ female mice was not sufficient to induce SLE (**Figure 2-figure supplement 3**). Nevertheless, both ACK1 and BRK inhibitors increased glomerular deposit of IgG in the kidney and serum autoantibodies levels including anti-Ku (p70/p80), LA/SSB, Ro-SSA, Histone H4 and H2B, in BALB/cByJ mice treated with pristane to induce a lupus-like disease [39], in comparison to treatment DMSO vehicle alone (**Figure 2F, G, Figure 2-figure supplement 3**). Therefore, inhibition of ACK1 and BRK worsen pristane-induced Lupus in WT mice, which is consistent with the genetic analysis indicating that autosomal recessive ACK1 and BRK kinase deficiency may underly or contribute to the development of SLE in children and young adults depending on genetic and environmental context.

ACK1 and BRK kinase domain variants may lose the ability to link MERTK to RAC1, AKT and STAT3 activation for efferocytosis.

NRTKs, including ACK1 and BRK, regulate phosphorylation of downstream effectors/ adaptor proteins involved in cell activation, migration, and proliferation including RAC1, AKT, STATs, and ERK [53,60-66]. NRTK deficiency can result in defective regulation of immune cell activation and survival which can lead to autoimmunity [36,37,40,67-71]. We found that, in contrast to the reference ACK1 and BRK alleles, the patient's ACK1 and BRK variant alleles do not phosphorylate AKT and STAT3 (**Figure 3A, B)**, and do not activate RAC1 to generate RAC-GTP (**Figure 3C**). NRTKs such as ACK1 [41] and PTK2/FAK [43] are also downstream targets of the TAM family receptor MERTK that controls the anti-inflammatory engulfment of apoptotic cells, a process known as efferocytosis [46,72,73]. Efferocytosis deficiency is associated with inflammation and autoimmunity [48,72,74-87]. In IP kinase assays MERTK activated the kinase activity of wild-type ACK1 [41] but not of the ACK1 A156T and ACK1 K161Q variant alleles (**Figure 3D**). In addition, MERTK also activated BRK kinase activity, but the BRK G321R and G257A alleles were kinase dead and hypomorph variants respectively (**Figure 3D**). MERTK mediates recognition of PtdSer on apoptotic cells via GAS6 and Protein S [46-48] leading to their engulfment, which involves activation of RAC1 for actin reorganization and the formation of a phagocytic cup [43,65]. PtdSer recognition also typically stimulates an anti-inflammatory process mediated in part via AKT [88] and STAT3 and their target genes such as SOCS3 [42,89-94] and results in the inhibition of LPS-mediated production of inflammatory mediators such as TNF and IL-1β, and the production of cytokines such as IL-10, TGFβ [72,85-87,95]. Altogether, these data raised the hypothesis that one of the consequences of the defective activity of ACK1 and BRK kinase variants might be an impaired efferocytic response to PtdSer on apoptotic cells.

ACK1 and BRK kinase deficiency disrupts the anti-inflammatory response driven by apoptotic cells in macrophages.

Efferocytosis can be carried out by multiple cell types, however macrophages are the main contributors in this process [92,96,97]. MERTK kinase activity mediates efferocytosis by human iPSC-derived macrophages [45], we thus examined the transcriptional responses of controls, patients, and inhibitor-treated iPSC-derived macrophages to apoptotic thymocytes by RNA-seq. GSEA analysis of differentially expressed genes indicated that, in contrast to control, ACK1- and BRK-deficient macrophages, as well as WT macrophages treated with ACK1 or BRK inhibitors failed to upregulate gene sets associated with AKT signaling and the negative regulation of the inflammatory response (**Figure 3E**). Transcriptional repressors including the AKT targets ATF3,

TGIF1, NFIL3, and KLF4, the STAT3 targets SOCS3 and DUSP5, as well as CEBPD and the inhibitor of E-BOX DNA Binding ID3 were among the top-ten genes which expression is induced by apoptotic cells in WT macrophages (**Figure 3F**), but this regulation was lost in mutant and inhibitor-treated macrophages (**Figure 3F**). ATF3, TGIF1, NFIL3, and KLF4 are involved in the negative regulation of inflammation in macrophages [89-92], SOCS3 is an inhibitor of the macrophage inflammatory response and DUSP5 is a negative regulator of ERK activation [93,94,98]. These data suggest that the kinase domain of ACK1 and BRK contribute to the macrophage anti-inflammatory gene expression program driven by apoptotic cells.

Decreased TNF gene expression by macrophages in response to apoptotic cells was prevented by the ACK1 inhibitor (**Figure 3G**), but the production of TNF at the protein level is not detectable by ELISA in this model (see **Figure 3H**). MERTK-deficient mice are susceptible to LPS-induced endotoxic shock [99], and MERTK-dependent anti-inflammatory program elicited by apoptotic cells on macrophages is best evidenced by the reduction of LPS-mediated production of inflammatory mediators such as TNF or IL-1b [85-88,99]. We thus tested the decrease of LPS-induced production of TNF and IL1b by apoptotic cells. For this purpose, we generated isogenic variants and control hiPSCs and hiPSCs-derived macrophages from the same donor (**Figure 3-figure supplement 1**). Both isogenic variants and control macrophages produced similar amounts of TNF in response to LPS (**Figure 3H**). However, exposure to apoptotic cells inhibited TNF production in isogenic macrophages by 50% but did not inhibit TNF production in ACK1 and BRK-deficient macrophages (**Figure 3H**). Similarly, isogenic variants and control macrophages produced similar amounts of IL1b in response to LPS (**Figure 3I**), but apoptotic cells only decreased IL1b production by isogenic macrophages and not by mutant macrophages (**Figure 3I**). These data altogether indicate that ACK1 and BRK kinase activities contribute to the macrophage anti-inflammatory response during efferocytosis and are required for the decrease of TNF and IL1b production induced by LPS in response to apoptotic cells, a hallmark of their anti-inflammatory effect on macrophages [72,85-87].

ACK1 and BRK kinase deficiency alter actin remodeling at the phagocytic cup and modestly decrease engulfment of apoptotic cells in macrophages.

MERTK-dependent signaling for anti-inflammatory response and for cargo engulfment driven by recognition of PtdSer on apoptotic cells are distinct and separable molecular events [44,100], however because RAC1, which controls engulfment of apoptotic cells [101], is a target of ACK1 and BRK (see **Figure 3C**) as well as PTK2/FAK [43], we investigated the engulfment of apoptotic cells by ACK1- and BRK-deficient macrophages. We assessed actin-ring formation by total internal reflection fluorescence (TIRF) microscopy in frustrated apoptotic engulfment assays on PtdSer-coated glass slides. Wild-type iPSC-derived macrophages formed a typical actin-ring, however isogenic ACK1 and BRK mutant macrophages presented with an altered actin-ring (**Figure 4A**), and a reduced actin clearance factor (**Figure 4B**), indicating an impairment of actin remodeling following binding to PtdSer. The actin-ring was also altered and actin clearance factor was decreased in WT macrophages treated with ACK1 and BRK inhibitors in comparison to controls (**Figure 4C,D**). These data suggest the kinase activity of ACK1 and BRK contributes to link PtdSer receptors to cytoskeleton rearrangement at the phagocytic synapse.

We therefore investigated whether this defect translated to a reduced uptake of apoptotic cells by macrophages. We found that engulfment of apoptotic thymocytes labeled with the pH sensitive probe pHrodo [97,102,103] was only moderately reduced, by 10 to 20% in ACK1 and BRK isogenic mutant macrophages (**Figure 4E)**. This phenotype, although modest, was reproducible

by a 30-minute exposure of WT macrophages to two different ACK1 inhibitors, Aim100 (2 μM) and R-9b [104] (4 μM), and to the BRK inhibitor Cpd4f (0.5 μM) (**Figure 4F).** This reduced uptake of apoptotic cells was not attributable to a global engulfment defect, because ACK1 and BRK genetic kinase deficiency or inhibitors did not prevent Fc-dependent phagocytosis of a large cargo such as opsonized red blood cells (**Figure 4G**), or the uptake of polystyrene beads (**Figure 4-figure supplement 1A)** or microorganisms such as bacteria and fungi (**Figure 4-figure supplement 1B, C)**. Altogether, these data show that the kinase activity of ACK1 and BRK participate to the formation of phagocytic synapse but are largely dispensable for engulfment of apoptotic cells and are not required for phagocytosis of microbes and opsonized cargo.

DISCUSSION

In this study we combined whole exome sequencing and forward genetic analysis in multiplex SLE families, with a biochemical analysis of genetic variants, murine studies, and functional approaches in human iPSC-derived macrophages to identify novel genes the mutations of which may underlie SLE. In two unrelated families, we identified compound heterozygous loss-of-function or hypomorph variants in the kinase domains of two non-receptors tyrosine kinases, TNK2/ACK1 and PTK6/BRK. Patients from the two families were children or young adults and presented with a severe clinical form of SLE, lupus nephritis. However, we analyzed 27 GWAS studies of SLE (https://www.gwascentral.org/), and none of them reported a common variant in the close vicinity of the TNK2/ACK1 or PTK6/BRK genes with a p-value lower than $5x10^{-8}$, a statistical threshold of genome-wide significance for GWAS. ACK1 and BRK deficiency are thus likely to only account for the genetic basis of SLE in a minority of patients. Nevertheless, ACK1 and BRK kinase inhibitors aggravate autoimmunity and IgG glomerular deposits in pristane-treated BALB/cByJ mice. Altogether, the present data indicate that autosomal recessive TNK2/ACK1 and PTK6/BRK kinase deficiency probably underlie the development of SLE in a small proportion of children and young adults, depending on genetic and environmental context.

Defective efferocytosis has been shown to contribute to autoimmunity in mice and is relevant to the pathogenesis of SLE [74-80,83,84]. Our results also suggest that TNK2/ACK1 and PTK6/BRK kinase deficiencies, in addition to dysregulating B and T cell survival and activation [36,37], also impairs the MERTK-dependent anti-inflammatory response of the patients' macrophages to apoptotic cells during efferocytosis, and to a lesser extent the engulfment of the apoptotic cells. Mertk-dependent engulfment of apoptotic cells and anti-inflammatory response were shown to be distinct and separable [44,100]. The NRTK PTK2/FAK and Src are important for the former [44,105], while PTK2/FAK is dispensable for the latter [44]. Our experiments suggest that in contrast, TNK2/ACK1 and PTK6/BRK are more important for the control of TNF and IL1b production than for engulfment itself. Altogether, our observations identify a rare Mendelian cause of severe SLE and a role for the NRTK TNK2/ACK1 and PTK6/BRK in efferocytosis, thereby contributing to a molecular and cellular dissection of SLE.

MATERIALS AND METHODS

Human sample collection and consent information

The study was approved by the Institutional Review Board of St Thomas' Hospital; Guy's hospital; the King's College London University and the Memorial Sloan Kettering Cancer Center. All subject samples were obtained after written informed consent from patients and their families according to the Helsinki convention (Ethics approval: 11/LO/1433). Ten multiplex families with lupus have been enrolled from Guy's and St Thomas' NHS Foundation Trust and UCL Hospital in London, UK from July 2010 to January 2012, following stringent criteria: a severe phenotype (lupus nephritis for at least 1 patient in each family), and a familial disease (≥2 family members affected in first degree). A total of 24 patients and 17 healthy controls from different ethnic origins (5 African ancestry, 4 Asian ancestry and 1 European ancestry) were selected. The patients each met the Systemic Lupus International Collaborating Clinics (SLICC) classification criteria for SLE[2]. Lupus nephritis was confirmed by a kidney biopsy classified per the 2004 ISN/RPS (International Society of Nephrology/Renal Pathology Society) classification and verified independently by 2 renal histopathologists.

One hundred Mauritian participants were enrolled under the Ethical Clearance provided by the University of Mauritius Research Ethics Committee. Written consent with due signatures was recorded from all participants prior to partaking in the study. Consent was documented on a confidential form in duplicate, with one copy given to the participants for their records. The University of Mauritius Research Ethics Committee approved, sanctioned and fully endorsed this mode of consent recording. The ethnic backgrounds of the 100 Mauritian participants consisted of 26 Creole, 16 Franco-Mauritian, 21 Indo-Mauritian, 2 Sino-Mauritian, 24 other or undisclosed Mauritians.

Genetic analysis.

Whole Exome Sequencing (WES) of the 10 multiplex families (patients and familial healthy controls) was performed at the New York Genomics Centre on an Illumina HiSeq 2000 sequencing machine. Genomic DNA extracted from the patients and familial healthy control's peripheral blood cells were sheared with a Covaris S2 Ultrasonicator. An adapter-ligated library was prepared with the Paired-End Sample Prep kit V1 (Illumina). Exome capture was performed with the SureSelect Human All Exon kit (Agilent Technologies). Paired-end sequencing was performed on a HiSeq 2000, generating 100-base reads. For sequence alignment, variant calling and annotation, we used BWA aligner[106] to align sequences with the human genome reference sequence (hg19 build). Downstream processing was performed with the Genome analysis toolkit[107], SAMtools[108], and Picard Tools. Substitution and indel calls were identified with a GATK Unified Genotyper and a GATK Indel GenotyperV2, respectively. All calls with a read coverage ≤2x and a Phred-scaled SNP quality of ≤20 were filtered out. All the variants were annotated with the GATK Genomic Annotator. Variants were annotated following their minor allele frequency (MAF) in Exome Variant Server, 1,000 Genomes Project, and Genome Aggregation Database (gnomAD), including the MAF in each ethnic subpopulation from gnomAD.

First, the variants have been prioritized at the gene level. We used the gene damage index (*GDI*) which provides the accumulated mutational damage of each human gene in healthy human population, based on the 1,000 Genomes Project database (Phase 3) gene variations of healthy individuals and of the CADD score for calculating impact[109]. GDI is very effective to filter out variants harbored in highly damaged (high GDI) genes that are unlikely to be disease-causing.

We used a cut-off of 13.84, the recommended GDI value above which a gene is unlikely to be disease-causing which is the 95% CI upper boundary value, removing 5% of the genes in our analysis.

Secondly, we prioritized variants at the allele level. We excluded variants that were too frequent in our in-house database to explain the disease[110]. We then filtered out variants based on the predicted damaging impacts. The deleteriousness of each variant was assessed using in silico algorithms: CADD (http://cadd.gs.washington.edu/score) and Mutation Significance Cutoff browser (MSC, http://pec630.rockefeller.edu/MSC/). MSC scores were generated using 99% confidence interval based on the CADD 1.3 scores of all disease causing-mutations in Human Gene Mutation Database for any given gene[54,55]. We kept only the variants with a CADD/MSC higher than 1.

We thus analyzed our WES with the remaining variants by keeping all non-synonymous coding variants and essential splice site variants with a MAF according to the genetic model: 1) heterozygous variations with MAF $<10^{-4}$ in all ethnic subpopulations under an autosomal dominant (AD) model; 2) homozygous or compound heterozygous variants with MAF $<10^{-2}$ in all ethnic subpopulations) under an autosomal recessive (AR) model; and 3) hemizygous (male) or homozygous (female) variations with MAF $<10^{-4}$ in all ethnic subpopulations under X-linked genetic models.

Principal component analysis

PCA was performed with 2,504 individuals of the 1,000 Genomes database using WES high quality variants as described in Belkadi et al. We searched for the closest neighbors of the patients in terms of ethnic origin using an Euclidian distance computed from the 10 first PCs [49,111].

Biochemical analysis

Cloning and Site-directed mutagenesis. The expression vectors for Flag- and HA-tagged Ack1 and for Flag-tagged Brk were described previously[52,112,113]. Site-directed mutagenesis was performed using the QuikChange Kit (Agilent; 200523). The expression vector for Cas has been described previously[114]. The expression vector for MerTK, pIRES2-EGFP Mer, was a gift from Dr. Raymond Birge[43].

Cell transfection, Immunoprecipitation, and Western Blotting. Cells were transfected 24 h after plating with 8 µL polyethylenimine per µg of DNA in 150 mM NaCl. Cells were harvested 48 h after transfection using lysis buffer (25 mM Tris, pH 7.5, 1 mM EDTA, 100 mM NaCl, 1% NP-40) supplemented with aprotinin, leupeptin, PMSF, and Na_3VO_4. For Western blotting, lysates were resolved by SDS-PAGE transferred to PVDF membranes, and probed with the appropriate antibodies. Horseradish peroxidase-conjugated secondary antibodies (GE Healthcare; NA931V; NA9340V) and Western blotting substrate (ThermoFisher Scientific; 32106) were used for detection. Phosphorylation of endogenous Cas is not as strong for BRK as it is for ACK1, so in these experiments we co-transfected with Cas and stimulated BRK by a 10 min 100 ng/ml EGF treatment[53].

For immunoprecipitation studies, cell lysates (1 mg total protein) were incubated with 1-2 µg of the appropriate antibody and 25 µL of protein A agarose (Roche; 11134515001) for at 4˚C for 4 h-overnight. Anti-Flag immunoprecipitations were done with anti-Flag M2 affinity resin (Sigma). The beads were washed three times with lysis buffer, then eluted with SDS-PAGE sample buffer and resolved by SDS-PAGE. The proteins were transferred to PVDF membrane for Western blot analysis.

Immunoprecipitation Kinase assay IP-kinase assays were carried out essentially as previously described[53]. Cell lysates (1 mg protein) were incubated with 25 µL of anti-Flag M2 affinity resin on a rotator for 4˚C for 4 h-overnight, then washed three times with Tris-buffered saline (TBS). A portion of each sample was eluted with SDS-PAGE sample buffer and analyzed by anti-Flag Western blotting. The remaining sample was used for a radioactive kinase assay. A WASP-derived peptide (sequence: KVIYDFIEKKKG)[115] was used as a substrate for Ack1, and a Src-specific peptide (sequence: AEEEEIYGEFEAKKKKG) [59,116] was used as a substrate for Brk. The immunoprecipitated proteins were incubated with 25 µL of reaction buffer (30 mM Tris, pH 7.5, 20 mM $MgCl_2$, 1 mg/mL BSA, 400 µM ATP), 1 mM peptide, and 50 – 100 cpm/pmol of [γ-^{32}P] ATP at 30˚C for 20 min. The reactions were terminated using 45 µL of 10% trichloroacetic acid. The samples were centrifuged and 30 µL of the reaction mixture was spotted onto Whatman P81 cellulose phosphate paper. After washing with 0.5% phosphoric acid, incorporation of radioactive phosphate into the peptide was measured by scintillation counting.

Rac binding assay The Cdc42/Rac interactive binding (CRIB) domain from PAK binds specifically to Rac in the GTP-bound state[117]. The PAK-CRIB domain was expressed as a GST fusion protein in E. coli and purified with glutathione-agarose. The immobilized CRIB domain was incubated with cell lysates (1 mg total protein) for 2h at 4˚C. The resin was washed with TBS, and bound proteins were eluted with SDS-PAGE sample buffer and analyzed by anti-Rac Western blotting.

Analysis of transcriptomics data for expression of TNK2 (ACK1) and PTK6 (BRK) in human and mouse cells.

Normalized expression data of TNK2 and PTK6 in human blood cells was extracted from Immgen RNASeq Database (Data Group: ULI RNA RNASeq) and plotted using Prism 8. Metadata on each cell type is shown in table 1.

Table 1 – Immgen Metadata of Human Blood Cells Dataset

Sample ID	Population Name	Organ	Cell Type	Description	TNK2 (DESeq2)	PTK6 (DESeq2)
1	B.NveIgD+27-.Bl	Blood	B	Sorted as CD19+ IgD+ CD27- PBMCs	260.437	51.1542
2	B.MemIgD-27+38-.Bl	Blood	B	Sorted as CD19+ IgD- CD27+ CD38- PBMCs	88.1885	14.3854
3	B.TransIgD+27+.Bl	Blood	B	Sorted as CD19+IgD+CD27- PBMCs	82.0064	11.3806
4	T.4Nve.CD3+4+RA+62L+.Bl	Blood	abT	Sorted as DR- TCRb+ CD4+ CD8- CD127+ CD25- CD54RAhi CD62Lhi PBMCs	88.4586	6.54898
5	T.4EffMem.CD3+4+RA-62L-.Bl	Blood	abT	Sorted as DR- TCRb+ CD4+ CD8- CD127+ CD54RA- CD62L- PBMCs	73.25	5.28517
6	T.8Nve.CD3+8+RA+62L+.Bl	Blood	abT	Sorted as DR- TCRb+ CD4- CD8+ CD127+ CD25- CD54RAhi CD62Lhi PBMCs	51.4156	6.63395
7	T.8EffMem.CD3+8+RA-62L-.Bl	Blood	abT	Sorted as DR- TCRb+ CD4- CD8+ CD127+ CD54RA- CD62L- PBMCs	60.3488	2.31369
8	T.NKT.Va24+.Bl	Blood	abT	Sorted as CD19- CD3+ XXX PBMCs	57.3267	1.47634
9	T.MAIT.4+.Bl	Blood	abT	Sorted as CD19- CD3+ CD4+ CD8- Va72.2+ CD161dull PBMCs	68.9702	5.01021
10	T.MAIT.8+.Bl	Blood	abT	Sorted as CD19- CD3+ CD4- CD8+ Va72.2+ CD161dull PBMCs	56.7917	11.139
11	T.Treg.rest.Bl	Blood	abT	Sorted as CD19- CD4- CD25+ CD127- CD45RA+ PBMCs	96.2381	2.05225

12	T.Treg.act.Bl	Blood	abT	Sorted as CD19- CD4- CD25+ CD127- CD45RA- PBMCs	53.4099	2.52522
13	ILC.Nkimm.56hi16-.Bl	Blood	ILC	Sorted as CD19- CD56hi PBMCs	57.2338	1.69447
14	ILC.Nkmat.56lo16hi57-.Bl	Blood	ILC	Sorted as CD19- CD56mid CD16+ CD57- PBMCs	72.9583	1.72836
15	ILC.Nkmem.56lo16hi57hi.Bl	Blood	ILC	Sorted as CD19- CD56mid CD16+ CD57+ PBMCs	73.6581	1
16	DC.DC1.141+.Bl	Blood	DC	Sorted as HLA.DR+ CD141+ CD16- CD14- PBMCs	88.7922	16.2214
17	DC.DC5.AXL+SIGLEC6+.Bl	Blood	DC	Sorted as HLA.DR+ CD141- CD16- CD14- AXL+ SIGLEC6+ PBMCs	114.054	23.6405
18	DC.DC6.123+.Bl	Blood	DC	Sorted as HLA.DR+ CD141- CD16- CD14- AXL- SIGLEC6- CD123+ CD11c- PBMCs	57.9988	1
19	Mo.16+.Bl	Blood	Mo	Sorted as HLA.DR+ CD16hi CD14lo PBMCs	100.41	19.9396
20	Mo.14+.Bl	Blood	Mo	Sorted as HLA.DR+ CD16lo CD14hi PBMCs	165.176	11.047

RNASeq data from sorted human microglia and brain tissue was extracted from available datasets [118,119]. Gene expression was log2 normalized. Data of normalized expression (CPM) of TNK2 and PTK6 in tSNE clustered cell populations of stromal vascular fraction from 10 healthy human subcutaneous adipose tissue samples was extracted and plotted using Single Cell Portal (The Broad Institute of MIT and Harvard), study: “Human Adipose SVF single cell”. Original data was provided by Beth Israel Deaconness Medical Center. Data of normalized expression of TNK2 and PTK6 in tSNE clustered cell populations in human ileal lamina propria was extracted and plotted using Single Cell Portal (The Broad Institute of MIT and Harvard), study: “ICA: Ileum Lamina Propria Immunocytes (Sinai)”[120]. Normalized expression (DESeq2) of TNK2 and PTK6 in mouse resident macrophages and monocytes was extracted from Immgen RNASeq Database (Data Group: ImmGen ULI RNASeq and ImmGen MNP OpenSource) and plotted using Prism 8.

Cells

HEK 293T

HEK 293T cells were maintained in Dulbecco’s modified Eagle’s medium (DMEM, Mediatech, Inc.) supplemented with 10% fetal bovine serum (FBS) (Sigma) and 1000 IU/ml penicillin and streptomycin.

Derivation of Human iPSCs

Generation of iPSCs from frozen peripheral blood mononuclear cells (PBMCs) was performed using a previously published protocol[121]. Briefly, PBMCs were cultured in QBSF-60 media supplemented with L-Asorbic Acid (50 µg/mL), human SCF (50 ng/mL) (R&D; 255-SC-010/CF), human IL-3 (10 ng/mL) (Peprotech; 200-03), human EPO (2 U/mL) (R&D; 287-TC-500), IGF-1 (40 ng/mL) (R&D; 291-G1-200), and Dexamethasone (1 µM) (Sigma; D8893-1MG) for 9 to 12 days to expand the erythroblast population. Then 4 Sendai viral vectors (ThermoFisher Scientific; A16517) expressing Oct3/4, Sox2, Klf4, or c-Myc are used for transduction of $2.5x10^5$ cells with 10 MOI for each virus for 24 hr. At day 2 post transduction, cells were plated in a 6 well gelatin coated plate containing MEFs (ThermoFisher Scientific; A34181). After 9-12 days, small iPSCs colonies appear. At day 17-21, several colonies were picked and expanded individually into 1 well (12-well or 24-well plate) containing MEFs on gelatin in ESC media as detailed above, supplemented with 10 ng/ml basic fibroblast growth factor (bFGF; Peprotech; 100-18B). Five clones were established per cell line and were maintained in culture for 10 passages (2-3 months) to ensure stability of the lines. Two clones per cell line were selected and tested for chromosomal

abnormality and showed a normal karyotype (46, XY or 46, XX). The other clones were frozen down.

Culture of Human iPSCs

Human induced Pluripotent Stem Cells (iPSCs) were maintained on mouse embryonic fibroblasts (MEFs, ThermoFisher Scientific; A34181) in ESC media (knock-out Dulbecco's modified Eagle medium (KO-DMEM, ThermoFisher Scientific; 10829-018) with 20% KO serum replacement (ThermoFisher Scientific; 10828-028), 2 mM L-glutamine (ThermoFisher Scientific; 25030-024), 1% nonessential amino acids (ThermoFisher Scientific; 11140-035), 1% penicillin/streptomycin (ThermoFisher Scientific; 15140-122), 0.2% β-mercaptoethanol (ThermoFisher Scientific; 31350-010) supplemented with 10 ng/ml basic fibroblast growth factor (bFGF, Peprotech; 100-18B). Passaging was performed every 7 days at 1:3-1:6 dilution ratio depending on the colony size. During passaging, iPSCs are detached as clusters by a 13 min incubation at 37°C with collagenase type IV (250 UI/ml final concentration) (ThermoFisher Scientific; 17104019) and are pelleted at room temperature by centrifugation at 100G. The iPSC clusters are resuspended in ESC medium supplemented with 10 ng/ml bFGF (Peprotech; 100-18B) and plated on NUNC plates containing 12,500 to 16,000 MEFs per cm^2.

Generation of the TNK2 (ACK1) and PTK6 (BRK) Isogenic Mutant iPSC lines.

CRIPSR and single-stranded donor oligonucleotides (ssODN) were used as the tool to introduce the SNP mutations in hiPSCs. CRISPR sgRNA target was designed using the web resource at https://www.benchling.com/crispr/. The target sequence was cloned into the pX330-U6-Chimeric_BB-CBh-hSpCas9 vector (Addgene plasmitd #42230) to make the gene targeting construct. The template ssODN was designed to carry the mutant nucleotide and served as the donor template. The ssODN was then purchased from IDT. The sgRNA-target and ssODN sequence are listed in Table 2.

To introduce the SNP mutations, WT iPSCs (C12) were dissociated using Accutase (Innovative Cell Technologies) and electroporated (1 $x10^6$ cells per reaction) with 4 µg sgRNA-construct plasmid and 4 µl ssODN (10 µM stock) using Human Stem Cell Nucleofector™ solution (Lonza) following manufacturer's instructions. The cells were then seeded, and 4 days later, hESCs were dissociated into single cells by Accutase and re-plated at a low density (4 per well in 96-well plates) to get the single-cell clones. 10 days later, individual colonies were picked, expanded and analyzed by PCR and DNA sequencing. The PCR and sequencing primers are listed in Table 3.

Table 2

	sgRNA target	ssODN
TNK2 (A156T/K161Q)	GGCTCAGGACATC GGGCTTC	GCAGGTTGGCTCCGCGTGTCTGGGACCTGGCAAGTCCTGAGTCCTTGCA AATCCCGCTCTGGGCAGGTGAGTGTGACTGTGAAGTGCCTGCAGCCCGA TGTCCTGAGCCAGCCAGAAGCCATGGACGACTTCATCCGGGAGGTCAA
PTK6 (G321R)	CGCCAGGAACATC CTCGTCG	GCTGAGGGCATGTGTTACCTGGAGTCGCAGAATTACATCCACCGGGACC TGGCCGCCAGGAACATCCTCGTCAGGGAAAACACCCTCTGCAAAGTTGG GGACTTCGGGTTAGCCAGGCTTATCAAGGTAGGGCCCTCAGAGGG

Table 3

	PCR-Forward primer (used for sequencing)	PCR-Reverse primer
TNK2	TGCTTACCCACCCAGATGAG	AAATCCAGAGACAGACCCGG
PTK6	GAGAAAGTCCTGCCCGTTTC	GATTGCAGGTGTGTGGGGA

Differentiation of iPSCs-derived macrophages.

The hiPSCs to macrophage differentiation method was adapted from a previously published protocol[58]. Briefly, newly passaged iPSCs were maintained from day 0 to day 3 in ESC media (see human iPSCs culture) with 10 ng/ml bFGF and from day 3 to day 7 in ESC media without bFGF. At day 7, iPSCs colonies were detached in clusters using collagenase type IV (250 UI/ml final concentration) (ThermoFisher Scientific; 17104019) and transferred to 6 well suspension plates in ESC media supplemented with 10 µM ROCK Inhibitor (Sigma; Y0503), on an orbital shaker at 100 rpm. The cell clusters were cultivated under these conditions from day 7 to day 13 to induce embryoid body (EB) formation. At day 13, well formed 200-500 µm EBs were manually picked under a microscope and transferred onto adherent tissue culture plates (~2.5 EBs/cm^2) for cultivation in APEL 2 medium (Stem Cell Tech; 05270) supplemented with 5% protein free hybridoma (ThermoFisher Scientific; 12040077), 100 IU/ml penicillin and 100 µg/ml streptomycin (ThermoFisher Scientific; 15140-122), 25 ng/ml human IL-3 (Peprotech; 200-03) and 50 ng/ml human M-CSF (Peprotech, 300-25). Starting from day 25 of the differentiation and then every week onwards for up to 5 weeks, suspension cells around EBs were carefully collected, filtered through a 100 µm mesh, plated at a density of ~15000 cells/cm^2, and cultivated for 6-10 days in RPMI1640/GlutaMax (ThermoFisher Scientific; 61870036) medium supplemented with 10% FBS (EMD Milipore TMS-013-B), and 100 ng/ml human M-CSF and used further for functional analysis. All cells were cultured at 37°C 5% CO_2 in standard tissue culture incubators.

Mice

C57BL/6J mice were used for preparation of apoptotic thymocytes and BALB/cByJ female were used for *in vivo* mouse inhibitor treatment (see below), and purchased from Jackson Laboratory. All mouse studies were performed in adherence with Institutional Review Board (IACUC 15-04-006 and 13-04-003) from MSKCC.

Antibodies and Flow cytometry

The following antibodies were used for human iPSCs-derived macrophages phenotyping: PE/Cy7 anti-human MERTK Ab (Biolegend; 367609); PE/Cy7 anti-human CD11b Ab (BioLegend; 301321); PE anti-human Intα5β3 Ab (R&D; FAB3050P); APC anti-human TIM4 Ab (BioLegend; 354007); AF647 anti-human TIM4 Ab (BioLegend; 354007); APC/Cy7 anti-human CD36 Ab (Biolegend; 336213); BV786 anti-human CD115 Ab (CSF-1R) (BD Biosciences; 743145); PE-Cy5 anti-human CD11c Ab (BD Biosciences; 561692); Alexa Fluor 700 anti-human HLA-DR Ab (BD Biosciences; 560743); APC/Cy7 anti-human CD45 Ab (BioLegend; 304014); BV650 anti-human CD14 Ab (BioLegend; 301836); Alexa Fluor 647 anti-human CD369 (Clec7A) Ab (BD Biosciences; 564855); Alexa Fluor 488 anti-human CD206 (MRC1) Ab (ThermoFisher Scientific; 564855)

iPSCs-derived macrophages were detached using trypsin (TrypLE Express, ThermoFisher Scientific; 12605-010, pelleted at 400g for 5 min and resuspended in fluorescence-activated cell sorting (FACS) buffer (PBS +0.5% bovine serum albumin (BSA) +1 mM EDTA). After blocking Fc receptors (Miltenyi; 130-059-901) at 1/10 dilution for 10 min, the cells were washed with FACS buffer, pelleted at 400G for 5 min, and immunostained in FACS buffer + antibody (1:50 to 1:200 dilution) for 30 min at 4°C. Data were acquired on an ARIA III BD flow cytometer or a FACS Fortessa SORP instrument and analyzed with FlowJo. Dead cells and debris were excluded from the analysis using DAPI (1 µg/ml), side (SSC-A) and forward scatter (FSC-A) gating, and doublet

exclusion using forward scatter width (FSC-W) against FSC-A. At least 5000 cells were acquired for each condition.

Cytology

Cells were collected into FBS and centrifuged (800 rpm, 8 min, low acceleration) onto Superfrost slides (ThermoFisher Scientific) using a Cytospin 3 (Thermo Shandon). Slides were air-dried for at least 30 min, and fixed for 5 min in methanol, stained in 50 % May-Grunwald solution for 15 min, 5% Giemsa for 15 min, washed with Sorensons buffered distilled water (pH 6.8) for 5 min and rinsed with Sorensons buffered distilled water (pH 6.8). Slides were air-dried and mounted with Entellan New (Merck) and representative pictures were taken using an Axio Lab.A1 microscope (Zeiss) under a N-Achroplan 100x/01.25 objective.

Engulfment of Beads, E. coli, or C. albicans by iPSC-macrophages

WT iPSCs-derived macrophages were plated at a density of 35,000 cells per well in 24 well plates, and maintained in 0.5 ml of RPMI containing 10% FBS. The macrophages were pretreated for 30 min with AIM100 (2 µM) and/or Cpd4f (0.5 µM) in RPMI without FBS prior to incubation with beads, E.coli or C. albicans.

Red fluorescent 2 µM Beads (Microparticles) (Invitrogen, F8826) were resuspended in RPMI ($5x10^5$ beads/ml), sonicated for 5 min, and part of the suspension was warmed to 37°C or cooled to 4°C. 400 µl of the suspension was added per well ($2x10^5$ beads/well) to pretreated iPSC-macrophages for each condition, and the plates were incubated for 1 h at 37°C or 4°C.

pHrodo E. coli BioParticles (Invitrogen, P35361) were resuspended in RPMI (0.5 mg/ml), sonicated for 5 min, and part of the suspension was warmed to 37°C or cooled to 4°C. 400 µl of the suspension was added per well (0.2 mg/well) to pretreated iPSC-macrophages for each condition, and the plates were incubated for 1 h at 37°C or 4°C.

Nonfluorescent and tdTomato positive C. albicans (clinical isolate SC5314) were grown overnight in YPD media at 30°C with 225 rpm shaking. The cells were washed with PBS, spun at 1000G for 5 min, and resuspended in RPMI to a density of 740,000 cells/ml. The suspensions were then warmed to 37°C or cooled to 4°C. 500 µl of the suspension was added per well (370,000 C. albicans cells) of iPSC-macrophages for each condition, and the plates were incubated for 1 h at 37°C or 4°C.

After the incubation with beads, E. coli or C. albicans, the media was removed and the wells were washed with PBS. The cells were then detached with a 3 min, 37°C incubation with trypsin, and collected by centrifugation at 400G for 5 min. The iPSC-macrophages incubated with beads or E. coli were resuspended in 200 µl of FACS buffer. The cells incubated with C. albicans were resuspended in PBS containing 20 µg/ml Calcofluor White (CFW) stain (Sigma), and were incubated for 15 min at room temperature to label unengulfed yeast. The cells were then washed with FACS buffer and pelleted at 400G for 5 min at 4°C, before being resuspended in 200 µl of FACS buffer.

The samples were analyzed using a FACS Fortessa SORP instrument. pHrodo Red and tdTomato fluorescence was detected through a 586/15 bandpass optical filter, on a 561nm laser excitation. CFW was excited by a 405 nm laser, and detected through a 495LP, 525/50 bandpass optical filters. At least two replicates were done for each condition.

Engulfment of murine apoptotic thymocytes and opsonized red blood cells.

Engulfment of apoptotic cells was assayed with pHrodo-labeled mouse apoptotic thymocytes as previously described[102,122]. Briefly, thymocytes from 4- to 8-week-old C57BL/6J mice were treated with Human leucine-zipper-tagged Fas ligand (FIZ-shFasL) (see below for preparation and concentration) in RPMI1640 containing 10% FBS for 2 h at 37°C to induce apoptosis, washed with PBS, and incubated with 0.1 µg/ml pHrodo for 30 min at room temperature. After the reaction was stopped with 1 ml FBS, the cells were washed with PBS containing 10% FBS and were used as prey.

Sheep red blood cells (MP Biomedicals, 0855876) were washed two times in PBS at 600G for 5 min, at room temperature. The cells were resuspended in PBS, counted and further diluted to a concentration of $1x10^8$ cells/ml. To opsonize the RBCs, 1/500 dilution of Rabbit Anti-Sheep RBC IgG (Cell Biolabs; 122001; CBA- 220) was added and the cells were incubated at 37°C for 30 min. The cells were then washed twice with PBS at 600G for 5 min, and stained in 1ml of PBS with 10 µg/ml pHrodo, under a 45 min incubation at room temperature. 1 ml of FBS was added to block the staining, and the cells were washed with PBS containing 10% FBS before being used in engulfment.

$0.5×10^6$ pHrodo-labeled apoptotic cells, or opsonized RBCs were added to 60 000 iPSCs-derived macrophages in 0.75 ml of RPMI containing 10% FBS in a 12-wells plate, and incubated at 37°C for 90 min. The cells were washed with PBS and detached with trypsin (TrypLE Express, ThermoFisher Scientific; 12605-010). The cells were collected by centrifugation at 400 g for 5 min, suspended in 300 µl of CHES (N-cyclohexyl-2-aminoethane- sulfonic acid)–fluorescence-activated cell sorter (FACS) buffer (20 mM CHES buffer [pH 9.0] containing 150 mM NaCl and 2% FBS) and analyzed by flow cytometry with a FACS Fortessa SORP instrument. At least 5000 cells were acquired for each condition. pHrodo was excited with the yellow green laser 561 nm and detected with 610/620 nm bandpass filter.

FIZ-shFasL was produced using HEK293T as described previously[103] and concentrated (around 50 fold) by ultrafiltration with Amicon Ultra-15 10K column (Sigma; UFC901008). The concentration used from each batch was determined with Alexa Fluor 488 Annexin V/Dead Cell Apoptosis Kit, as the concentration for which more than 80% of cells were annexin V positive and less than 10% propidium iodide positive.

Frustrated phagocytosis assay and TIRF imaging

Supported lipid bilayers containing 1,2-dioleoyl-sn-glycero-3-phospho-L-serine (DOPS; Avanti Polar Lipids, 840035) were prepared as previously described [123]. Cells were incubated on bilayers (20 min, 37°C) and fixed by adding 3% paraformaldehyde (20 min). Fixed cells were permeabilized with 0.2% Triton X-100 (15 min) and blocked in 10% goat serum/PBS (1 hr). Then cells were incubated with the phospho-Cas (Tyr165) antibody (Cell Signaling; 4015) (16 h, 4°C), washed, and incubated with the Alexa Fluor 488 goat anti-rabbit secondary antibody and 0.1 U/ml Alexa Fluor 594–labeled phalloidin (ThermoFisher Scientific; A12381) (1 hr, room temperature).

TIRF images of fluorescently labeled cells in contact with bilayers were collected with a 60× objective lens (1.45 NA; Olympus) using 488 and 561 nm lasers (Melles Griot) for imaging of Phospho-CAS (Cell signaling; Cat#4015) and Phalloidin (ThermoFisher Scientific; Cat#A12381), respectively.

Phospho-CAS intensity was calculated as the background-corrected mean fluorescence intensity (MFI) in every cell area, manually drawn using SlideBook software (3I). Quantification of clearance ratio was performed with Matlab software (Mathworks) from the TIRF images of background-corrected MFI as previously described[124]. Briefly, using two perpendicular linescans

for each cell, the background-corrected MFI at the edges (positions F1 and F2) of the IS was compared with the background-corrected MFI of three equally spaced central positions (F3, F4, and F5) as follows: mean (F3 + F4 + F5) / mean (F1 + F2). Clearance ratios derived from the two-perpendicular line- scans were averaged to yield a clearance ratio for the cell in question.

Transcriptomic analysis by RNA-seq

70,000 iPSCs-derived macrophages were plated per well in 12 well plates in RPMI1640/GlutaMax medium supplemented with 10% FBS, and 100 ng/ml human M-CSF. WT and mutants (ACK1A156T/K161Q and BRKG257A/G321R) iPSCs-derived macrophages were co-incubated or not with 450,000 mouse apoptotic thymocytes (as described above) in RPMI for 90 min. WT iPScs-derived macrophages were also pretreated for 30 min with AIM100 (2 µM) or cpd4f (0.5 µM) in RPMI and then incubated or not with mouse apoptotic thymocytes. Every condition was done in duplicate or triplicate. After 90 min incubation media was removed and macrophages were washed once with PBS. Then 1 ml TRIzol (ThermoFisher Scientific; 15596018) was added per well and cells were harvested and stored at -80°C. RNA from cells suspended in TRIzol was extracted with chloroform. Isopropanol and linear acrylamide were added, and the RNA was precipitated with 75% ethanol. Sample were resuspended in RNase-free water.

Transcriptome sequencing After RiboGreen quantification and quality control by Agilent Bioanalyzer, 65.8-100 ng of total RNA underwent polyA selection and TruSeq library preparation according to instructions provided by Illumina (TruSeq Stranded mRNA LT Kit; RS-122-2102), with 8 cycles of PCR. Samples were barcoded and run on a HiSeq 4000 or HiSeq 2500 in rapid mode in a 50bp/50bp paired end run, using the HiSeq 3000/4000 SBS Kit or HiSeq Rapid SBS Kit v2 (Illumina). An average of 50 million paired reads was generated per sample. At the most the ribosomal reads represented 7.1% of the total reads generated and the percent of mRNA bases averaged 80.4%.

Analysis The output data (FASTQ files, see below) were mapped to the target genome using the rnaStar aligner[125] that both maps reads to the genome and resolves reads that map across splice junctions. We used the 2 pass mapping method outlined as described[126], in which the reads are mapped twice. The first pass used a list of known annotated junctions from Ensemble. Novel junctions found in the first pass are then added to the list of known junctions and then a second mapping pass is done (on the second pass the RemoveNoncanoncial flag is used). After mapping we post process the output SAM files using the PICARD tools to: add read groups, AddOrReplaceReadGroups which in addition sorts the mapped reads by coordinates and coverts the file to the compressed BAM format. We then compute the expression count matrix from the mapped reads using HTSeq (www-huber.embl.de/users/anders/HTSeq) using Genecode v18 database for gene models. The raw count matrix generated by HTSeq was then processed using the R/Bioconductor package DESeq (www-huber.embl.de/users/anders/DESeq) which was used to both normalize the full dataset and analyze differential expression between sample groups.

The hypergeometric test and Gene Set Enrichment Analysis (GSEA)[127] was used to identify enriched signatures using the different pathways collection in the MSigDB database[128]. We used GSEA pre-ranked method from GSEA for our purpose.

FASTQFileID	conditions
C12-1_IGO_08681_C_13	Ctrl
C12-3_IGO_08681_C_15	Ctrl
C12-Acs-1_IGO_08681_C_16	Ctrl+ apop cells
C12-Acs-2_IGO_08681_C_17	Ctrl+ apop cells
C12-Acs-3_IGO_08681_C_18	Ctrl+ apop cells
C12-AIM100-1_IGO_08681_C_19	Ctrl+ACK1 inhib
C12-AIM100-2_IGO_08681_C_20	Ctrl+ACK1 inhib
C12-AIM100-Acs-1_IGO_08681_C_23	Ctrl+ACK1 inhib+apop cells
C12-AIM100-Acs-2_IGO_08681_C_24	Ctrl+ACK1 inhib+apop cells
C12-AIM100-Acs-3_IGO_08681_C_25	Ctrl+ACK1 inhib+apop cells
C12-Cpd4f-1_IGO_08681_C_21	Ctrl+BRK inhib
C12-Cpd4f-2_IGO_08681_C_22	Ctrl+BRK inhib
C12-Cpd4f-Acs-1_IGO_08681_C_26	Ctrl+BRK inhib+apop cells
C12-Cpd4f-Acs-2_IGO_08681_C_27	Ctrl+BRK inhib+apop cells
F1A-1_IGO_08681_C_1	ACK1 KO patient
F1A-2_IGO_08681_C_2	ACK1 KO patient
F1A-3_IGO_08681_C_3	ACK1 KO patient
F1A-Acs-1_IGO_08681_C_4	ACK1 KO patient+apop cells
F1A-Acs-2_IGO_08681_C_5	ACK1 KO patient+apop cells
F1A-Acs-3_IGO_08681_C_6	ACK1 KO patient+apop cells
F9A-1_IGO_08681_C_28	BRK KO patient
F9A-2_IGO_08681_C_29	BRK KO patient
F9A-3_IGO_08681_C_30	BRK KO patient
F9A-ACs-1_IGO_08681_C_31	BRK KO patient+apop cells
F9A-ACs-2_IGO_08681_C_32	BRK KO patient+apop cells
F9A-ACs-3_IGO_08681_C_33	BRK KO patient+apop cells
ACs_IGO_08681_C_46	mouse apoptotic thymocytes alone

Quantitative RT-PCR

Total RNA was extracted from cells using a quick-RNA Microprep kit (Zymo research; R1050) as per manufacturer's instructions. RNA was extracted from 150,000 iPSCs-derived macrophages in 6 well plates or 37500 iPSCs-derived macrophages in 24 well plates depending on the quantity of RNA needed. Lysis buffer was added directly in the well after 1 wash with PBS, then RNA was extracted directly or cells in lysis buffer were stored at -80°C. cDNA preparation was performed with Quantitect Reverse transcription kit (Qiagen; 205313) as per manufacturer instructions. qRT-PCR are done with 20 ng cDNA. qRT-PCR are performed on a Quant Studio 6 Flex using TaqMan Fast Advance Mastermix (ThermoFisher Scientific; 4444557), and TaqMan probes for GAPDH (Hs02758991_m1), TIMD4 (Hs00293316_m1), MERTK (Hs01031973_m1), ITGB5 (Hs00174435_m1), ITGB1 (Hs01127536_m1), ITGB3 (Hs01001469_m1), TNK2 (Hs01006880_m1), PTK6 (Hs00966641_m1), TNF (Hs00174128_m1). Comparative threshold cycles (CT) was used to determine gene expression. For each sample, genes CT value were normalized with the formula ΔCT = CTgene − CTGAPDH. For relative expression, the mean ΔCT was determined, and relative gene expression was calculated with the formula 2^(−ΔCT).

TNF-alpha and IL-1-beta ELISA

hiPSC macrophages plated in 24 well tissue culture plates (density of 15000 cells/cm2) were co-cultured with or without apoptotic thymocytes (1/8 mac./apop.t. ratio) for 90 min at 37C in complete media (RPMI, 10% FBS, 100ng/ml M-CSF). The wells were then washed once with PBS at 37°C to remove the majority of remaining apoptotic thymocytes. 300ul of complete media with or without 1ng/ml LPS was added in each well and the cells were incubated for 18hrs at 37C in a CO_2 incubator. The media was then collected and stored at -80C. ELISA was conducted according to manufacturer's protocol (Human TNF-alpha DuoSet (R&D; DY210) and IL1b DuoSet (R&D, DY201) ELISA kit).

Engulfment of apoptotic thymocytes by murine thioglycolate-elicited peritoneal macrophages *in vitro*.

To prepare thioglycolate-elicited peritoneal macrophages, 8-12 week-old mice were injected intraperitoneally with 2ml of 3% thioglycolate medium. Peritoneal exudate cells (PEC) were harvested 4 days after injection in PBS, washed and resuspended in DMEM 10% FCS. The cells were plated in 24 well tissue culture plates (120,000 cells/well) and incubated for 3 hrs at 37C in a CO_2 incubator.

Before co-incubation with murine apoptotic thymocytes, the cells were washed with PBS and incubated with the indicated concentrations of R9-B or Cpd4f for 30 min. After 30 min, the cells were washed and incubated with 10x apoptotic thymocytes in DMEM with 10% FBS for 90 min. The cells were washed, detached (5min incubation with Trypsin EDTA, followed by scraping) and resuspended in CHES-buffer (pH 9.0) containing 150 mM NaCl and 2% FCS, and anti-mouse-CD11b–PEcy7 antibody.

***In Vivo* Mouse Inhibitor and Pristane Treatment, Serum Preparation, and Kidney Fixation.**

Five week-old BALB/cByJ female mice received intra-peritoneal injection of DMSO (vehicle, 20 µl/mice), AIM100 (25 mg/kg in 20 µl), or Cpd4f (20 mg/kg in 20 µl) for 3 months. Injection were administered biweekly for the first 5 weeks, and weekly subsequently. The mice received a single intraperitoneal injection of PBS (500ul) or pristane oil (Sigma, P9622) (500ul) when 7 weeks old. Blood was collected by cardiac puncture. To collect serum, the blood was left to clot, undisturbed at room temperature for 30 min. The samples were then centrifuged at 1500G for 10 min at 4°C and the supernatant/serum was collected and stored at -80°C. The kidneys were removed, washed with PBS at 4°C, and were fixed whole in 4% PFA overnight at 4°C. The kidneys were then washed with PBS and place in 15% sucrose at 4°C for 3.5hrs. The kidneys were transferred in 30% sucrose and incubated overnight at 4°C. The kidneys were then dried with kimwipes and embedded in blocks in frozen section compound (Leica Ref:3801480). The blocks were placed in dry ice ethanol bath to freeze and were transferred to -80°C for storage.

Kidney Histology and Image Analysis

Frozen kidneys were sectioned longitudinally into 12um sections and transferred on glass slides. The sections were left to dry for 20-30minutes at room temperature (RT) and were transferred for storage at -20°C. To stain, the sections were thawed at RT for 15 minutes in a humidified box, and rehydrated by washing in PBS at RT 3 times. The sections were incubated for 1hr at RT in PBS, 5% BSA to block. The sections were then washed 2 times with PBS at RT and stained overnight at 4°C with IgG AF555 (Goat Anti-Mouse; ThermoFisher A21424) (1/500 dilution in PBS, 0.5% BSA), and Podoplanin (Syrian Hamster Anti-Mouse; Biolegend 127401) (1/100 dilution in PBS, 0.5% BSA). The sections were washed with PBS at RT 3 times and were incubated for 1.5hrs at RT with Anti-Syrian Hamster AF647 (Jackson, 107-605-142) (1-500 in PBS, 0.5% BSA). The sections were washed with PBS at RT 3 times and stain with Hoechst (ThermoFisher 62249) (20uM final concentration in PBS) for 10 min at room temperature. The slides were washed with PBS 2 times, and mounted using 170ul of ProLong Gold antifade reagent (Invitrogen P36930) and high precision microscope cover glass (24X50mm; 170uM; No. 1.5H). Entire kidneys sections were imaged on confocal microscope with 10X objective.

To analyze IgG mean fluorescence intensity (MFI) of glomeruli, podoplanin staining was used to algorithmically generate outlines around glomeruli in full kidney section images using ImageJ. The outlines were manually verified to remove incorrectly marked glomeruli and to outline the glomeruli the algorithm missed. Over 95% of all the glomeruli in a section (about 250 per whole longitudinal kidney section) were captured and analyzed for each mice (5 mice were analyzed for

each condition (30 whole kidney sections in total)). The MFI of each outlined glomeruli was extracted with ImageJ.

Autoantigen Microarray Panel Profiling

For each sample, 10 µl of serum was treated with DNAse I, diluted 1:50, and incubated with autoantigen array. The autoantibodies binding to the antigens on the array were detected with Cy3 labeled anti-IgG. The arrays were scanned with GenePix® 4400A Microarray Scanner and the images were analyzed using GenePix 7.0 software to generate GPR files. The averaged net fluorescent intensity (NFI) of each autoantigen was normalized to internal (IgG) controls. Plotted values represent Ab Scores (Log_2 [antigen net fluorescence intensity (NFI) x signal to noise ratio (SNR)+1]. Heatmaps were plotted with Morpheus (https://software.broadinstitute.org/morpheus/). Heatmap rows were sorted top to bottom starting with most significantly increased Ab Score in Cpd4f and AIM100 in comparison to DMSO treated mice. Single row P value between DMSO and Cpd4f or AIM100 mice was calculated by paired t test. Full panel P-values were calculated using a paired t test. Hierarchical clustering was done by one minus Pearson correlation with complete linkage method. K Means clustering was done by Euclidean distance, with 2 clusters, with 10000 maximum iterations.

Quantification and Statistical Analysis

Data are shown as mean with individual values or as bar plots with mean values and standard deviations. Statistical significance was analyzed with GraphPad Prism unless otherwise indicated (see below). For comparison between two groups we used unpaired t-test and for comparison between multiple groups we used ordinary one-way ANOVA (Tukey's multiple comparisons test) as indicated in the figure legends. Data were judged to be statistically significant when $p< 0.05$, and are reported in the figures. R software was used for statistical analysis of RNA-seq data. For differential gene expression approach significance was considered for FDR (q value) < 0.05. For gene set enrichment analysis (GSEA) approach significance was considered for FDR (q value) < 0.25 AND p-value < 0.05.

Data and materials availability: Genealogy trees of the 10 multiplex families recruited, clinical features of the 22 lupus patients recruited from 10 kindreds, and clinical features of the patients in ACK1 and BRK families can be requested from the corresponding author. Raw data files for the RNA sequencing analysis have been deposited in the NCBI Gene Expression Omnibus under accession number GEO: GSE118730.

Contact for reagent and resource sharing: Further information and request for reagents may be directed to and will be fulfilled by the corresponding author Frederic Geissmann: geissmaf@mskcc.org.

ACKNOWLEDGEMENTS

General: We are grateful to Ingeborg Bajema and Suzanne Wilhelmus from Leiden University Medical Center and Terry Cook from Imperial College Healthcare NHS trust London for help with the pathological review of patients, and Louise Nel from Guy's and St Thomas' NHS Foundation Trust for taking care of the patients.

Funding: We acknowledge the use of the MSKCC Stem Cell Research Core and MSKCC Integrated Genomics Operation Core, funded by the NCI Cancer Center Support Grant (CCSG, P30 CA08748), Cycle for Survival and the Marie-Josée and Henry R. Kravis Center for Molecular Oncology. This work was supported by National Cancer Institute of the US National Institutes of Health (P30CA008748) MSKCC core grant and grants from Ludwig Institute for Cancer Research and NIH/NIAID 1R01AI130345-01 and 5R01AI124349-03 (to FG) NIH/NIAID R01-AI087644 (to MH), NIH/NCI CA58530 (to WTM), NIH/NIAID R01-AI087644 to MH, and Grants-in-Aid for Scientific Research (S) from JSPS (No. 15H05785) and Core Research for Evolutional Science and Technology from Japan Science and Technology Agency (JPMJCR14M4) (to SN). SG was supported by Fellowships from the Fondation pour la Recherche Medicale (DEA20140630127), the European Federation of Internal medicine (EFIM), the Assistance Publique-Hopitaux de Paris (Annee Recherche), and from Institut Servier. NJ was supported by Fellowships from the Arthritis Research UK Fellowship and Graham Hughes Clinical Research Fellowship; her present address: Rheumatology Department, Cambridge University Hospitals, Hills Road, Cambridge, CB2 0QQ, UK.

Author contributions: FG designed the study. SG, TL and FG wrote the manuscript and prepared figures. NJ, DDC and DI selected patients and collected DNA and cell samples. SG, BB, LA, and JLC performed and analyzed exome sequencing. SDD and RIFL collected and performed exome sequencing of Mauritian participants. NL provided background in iPSC generation and macrophage differentiation. WTM and BC performed and analyzed biochemistry experiments. TZ and TL generated the isogenic CRISPR-CAS9 mutant iPSC lines. TL and SG performed iPSC culture, macrophage differentiation, phagocytosis and efferocytosis assays, flow cytometry, microscopy, qPCR and ELISA experiments, and analyzed mice, with help from HY. SG, MT, MH, and TL performed and analyzed frustrated phagocytosis assays with support from ELM. SG, RB, and OE performed RNA-seq experiments and primary and differential analysis of the RNA-seq data. CN and SN provided essential reagents and protocols for efferocytosis assays. AV and NDS supervised RNA-sequencing. All authors contributed to the manuscript.

Competing interest: Authors declare no competing interests

REFERENCES

1 Dall'Era, M. in *Current Rheumatology Diagnosis and Treatment. 3rd ed.* (eds J.B. Imboden, D.B. Hellman, & J.H. Stone) (McGraw-Hill, 2013).

2 Petri, M. *et al.* Derivation and validation of the Systemic Lupus International Collaborating Clinics classification criteria for systemic lupus erythematosus. *Arthritis Rheum* **64**, 2677-2686 (2012). https://doi.org:10.1002/art.34473

3 Rees, F., Doherty, M., Grainge, M. J., Lanyon, P. & Zhang, W. The worldwide incidence and prevalence of systemic lupus erythematosus: a systematic review of epidemiological studies. *Rheumatology* **56**, 1945–1961 (2017). https://doi.org:10.1093/rheumatology/kex260

4 Johnson, A. E., Gordon, C., Palmer, R. G. & Bacon, P. A. The prevalence and incidence of systemic lupus erythematosus in Birmingham, England. Relationship to ethnicity and country of birth. *Arthritis Rheum* **38**, 551-558 (1995). https://doi.org:10.1002/art.1780380415

5 Feldman, C. H. *et al.* Epidemiology and sociodemographics of systemic lupus erythematosus and lupus nephritis among US adults with Medicaid coverage, 2000-2004. *Arthritis Rheum* **65**, 753-763 (2013). https://doi.org:10.1002/art.37795

6 Somers, E. C. *et al.* Population-based incidence and prevalence of systemic lupus erythematosus: the Michigan Lupus Epidemiology and Surveillance program. *Arthritis Rheumatol* **66**, 369-378 (2014). https://doi.org:10.1002/art.38238

7 Lim, S. S., Bayakly, A. R., Helmick, C. G., Gordon, C., Easley, K. A. & Drenkard, C. The incidence and prevalence of systemic lupus erythematosus, 2002-2004: The Georgia Lupus Registry. *Arthritis Rheumatol* **66**, 357-368 (2014). https://doi.org:10.1002/art.38239

8 Ferucci, E. D. *et al.* Prevalence and incidence of systemic lupus erythematosus in a population-based registry of American Indian and Alaska Native people, 2007-2009. *Arthritis Rheumatol* **66**, 2494-2502 (2014). https://doi.org:10.1002/art.38720

9 Chakravarty, E. F., Bush, T. M., Manzi, S., Clarke, A. E. & Ward, M. M. Prevalence of adult systemic lupus erythematosus in California and Pennsylvania in 2000: estimates obtained using hospitalization data. *Arthritis Rheum* **56**, 2092-2094 (2007). https://doi.org:10.1002/art.22641

10 Hoi, A. Y. & Morand, E. F. Treatment Update in Systemic Lupus Erythematous. *Rheumatic Disease Clinics of North America* **47**, 513-530 (2021). https://doi.org:https://doi.org/10.1016/j.rdc.2021.04.012

11 Tektonidou, M. G., Dasgupta, A. & Ward, M. M. Risk of End-Stage Renal Disease in Patients With Lupus Nephritis, 1971-2015: A Systematic Review and Bayesian Meta-Analysis. *Arthritis Rheumatol* **68**, 1432-1441 (2016). https://doi.org:10.1002/art.39594

12 Menez, S. P., El Essawy, B. & Atta, M. G. Lupus Nephritis: Current Treatment Paradigm and Unmet Needs. *Rev Recent Clin Trials* **13**, 105-113 (2018). https://doi.org:10.2174/1574887112666171123113200

13 Hanly, J. G. *et al.* The frequency and outcome of lupus nephritis: results from an international inception cohort study. *Rheumatology (Oxford)* **55**, 252-262 (2016). https://doi.org:10.1093/rheumatology/kev311

14 Parikh, S. V., Almaani, S., Brodsky, S. & Rovin, B. H. Update on Lupus Nephritis: Core Curriculum 2020. *American journal of kidney diseases : the official journal of the*

National Kidney Foundation **76**, 265-281 (2020). https://doi.org:10.1053/j.ajkd.2019.10.017

15 Arnett, F. C. & Shulman, L. E. Studies in familial systemic lupus erythematosus. *Medicine (Baltimore)* **55**, 313-322 (1976). https://doi.org:10.1097/00005792-197607000-00003

16 Alarcon-Segovia, D. *et al.* Familial aggregation of systemic lupus erythematosus, rheumatoid arthritis, and other autoimmune diseases in 1,177 lupus patients from the GLADEL cohort. *Arthritis Rheum* **52**, 1138-1147 (2005). https://doi.org:10.1002/art.20999

17 Reichlin, M., Harley, J. B. & Lockshin, M. D. Serologic studies of monozygotic twins with systemic lupus erythematosus. *Arthritis Rheum* **35**, 457-464 (1992). https://doi.org:10.1002/art.1780350416

18 Deapen, D. *et al.* A revised estimate of twin concordance in systemic lupus erythematosus. *Arthritis Rheum* **35**, 311-318 (1992). https://doi.org:10.1002/art.1780350310

19 Belot, A. *et al.* Protein kinase cdelta deficiency causes mendelian systemic lupus erythematosus with B cell-defective apoptosis and hyperproliferation. *Arthritis Rheum* **65**, 2161-2171 (2013). https://doi.org:10.1002/art.38008

20 Kiykim, A. *et al.* Potentially Beneficial Effect of Hydroxychloroquine in a Patient with a Novel Mutation in Protein Kinase Cdelta Deficiency. *J Clin Immunol* **35**, 523-526 (2015). https://doi.org:10.1007/s10875-015-0178-9

21 Salzer, E. *et al.* B-cell deficiency and severe autoimmunity caused by deficiency of protein kinase C delta. *Blood* **121**, 3112-3116 (2013). https://doi.org:10.1182/blood-2012-10-460741

22 Al-Mayouf, S. M. *et al.* Loss-of-function variant in DNASE1L3 causes a familial form of systemic lupus erythematosus. *Nat Genet* **43**, 1186-1188 (2011). https://doi.org:10.1038/ng.975

23 Ozcakar, Z. B. *et al.* DNASE1L3 mutations in hypocomplementemic urticarial vasculitis syndrome. *Arthritis Rheum* **65**, 2183-2189 (2013). https://doi.org:10.1002/art.38010

24 Sisirak, V. *et al.* Digestion of Chromatin in Apoptotic Cell Microparticles Prevents Autoimmunity. *Cell* **166**, 88-101 (2016). https://doi.org:10.1016/j.cell.2016.05.034

25 Teruel, M. & Alarcon-Riquelme, M. E. The genetic basis of systemic lupus erythematosus: What are the risk factors and what have we learned. *J Autoimmun* **74**, 161-175 (2016). https://doi.org:10.1016/j.jaut.2016.08.001

26 Pickering, M. C., Botto, M., Taylor, P. R., Lachmann, P. J. & Walport, M. J. Systemic lupus erythematosus, complement deficiency, and apoptosis. *Adv Immunol* **76**, 227-324 (2000). https://doi.org:10.1016/s0065-2776(01)76021-x

27 Winkelstein, J. A. *et al.* Chronic granulomatous disease. Report on a national registry of 368 patients. *Medicine (Baltimore)* **79**, 155-169 (2000).

28 Foster, C. B. *et al.* Host defense molecule polymorphisms influence the risk for immune-mediated complications in chronic granulomatous disease. *J Clin Invest* **102**, 2146-2155 (1998). https://doi.org:10.1172/JCI5084

29 van den Berg, J. M. *et al.* Chronic granulomatous disease: the European experience. *Plos One* **4**, e5234 (2009). https://doi.org:10.1371/journal.pone.0005234

30 Ling, G. S. *et al.* C1q restrains autoimmunity and viral infection by regulating CD8(+) T cell metabolism. *Science* **360**, 558-563 (2018). https://doi.org:10.1126/science.aao4555

31 Bader-Meunier, B. *et al.* Are RASopathies new monogenic predisposing conditions to the development of systemic lupus erythematosus? Case report and systematic review of the literature. *Semin Arthritis Rheum* **43**, 217-219 (2013). https://doi.org:10.1016/j.semarthrit.2013.04.009

32 Jeremiah, N. *et al.* Inherited STING-activating mutation underlies a familial inflammatory syndrome with lupus-like manifestations. *J Clin Invest* **124**, 5516-5520 (2014). https://doi.org:10.1172/JCI79100

33 Crow, Y. J. *et al.* Characterization of human disease phenotypes associated with mutations in TREX1, RNASEH2A, RNASEH2B, RNASEH2C, SAMHD1, ADAR, and IFIH1. *Am J Med Genet A* **167A**, 296-312 (2015). https://doi.org:10.1002/ajmg.a.36887

34 Lee-Kirsch, M. A. *et al.* Mutations in the gene encoding the 3'-5' DNA exonuclease TREX1 are associated with systemic lupus erythematosus. *Nat Genet* **39**, 1065-1067 (2007). https://doi.org:10.1038/ng2091

35 Ramantani, G. *et al.* Aicardi-Goutieres syndrome and systemic lupus erythematosus (SLE) in a 12-year-old boy with SAMHD1 mutations. *J Child Neurol* **26**, 1425-1428 (2011). https://doi.org:10.1177/0883073811408310

36 Kasprzycka, M. *et al.* Expression and oncogenic role of Brk (PTK6/Sik) protein tyrosine kinase in lymphocytes. *The American journal of pathology* **168**, 1631-1641 (2006). https://doi.org:10.2353/ajpath.2006.050521

37 Sridaran, D. *et al.* Inhibiting ACK1-mediated phosphorylation of C-terminal Src kinase counteracts prostate cancer immune checkpoint blockade resistance. *Nature communications* **13**, 6929 (2022). https://doi.org:10.1038/s41467-022-34724-5

38 Haegebarth, A. *et al.* Protein tyrosine kinase 6 negatively regulates growth and promotes enterocyte differentiation in the small intestine. *Molecular and cellular biology* **26**, 4949-4957 (2006). https://doi.org:10.1128/MCB.01901-05

39 Satoh, M. & Reeves, W. H. Induction of lupus-associated autoantibodies in BALB/c mice by intraperitoneal injection of pristane. *The Journal of Experimental Medicine* **180**, 2341-2346 (1994). https://doi.org:10.1084/jem.180.6.2341

40 Yu, C. C., Yen, T. S., Lowell, C. A. & DeFranco, A. L. Lupus-like kidney disease in mice deficient in the Src family tyrosine kinases Lyn and Fyn. *Curr Biol* **11**, 34-38 (2001).

41 Mahajan, N. P., Whang, Y. E., Mohler, J. L. & Earp, H. S. Activated tyrosine kinase Ack1 promotes prostate tumorigenesis: role of Ack1 in polyubiquitination of tumor suppressor Wwox. *Cancer Res* **65**, 10514-10523 (2005). https://doi.org:10.1158/0008-5472.CAN-05-1127

42 Yi, Z., Li, L., Matsushima, G. K., Earp, H. S., Wang, B. & Tisch, R. A novel role for c-Src and STAT3 in apoptotic cell-mediated MerTK-dependent immunoregulation of dendritic cells. *Blood* **114**, 3191-3198 (2009). https://doi.org:10.1182/blood-2009-03-207522

43 Wu, Y., Singh, S., Georgescu, M. M. & Birge, R. B. A role for Mer tyrosine kinase in alphavbeta5 integrin-mediated phagocytosis of apoptotic cells. *J Cell Sci* **118**, 539-553 (2005). https://doi.org:10.1242/jcs.01632

44 Tibrewal, N. *et al.* Autophosphorylation docking site Tyr-867 in Mer receptor tyrosine kinase allows for dissociation of multiple signaling pathways for phagocytosis of apoptotic cells and down-modulation of lipopolysaccharide-inducible NF-kappaB transcriptional activation. *J Biol Chem* **283**, 3618-3627 (2008). https://doi.org:10.1074/jbc.M706906200

45 Wanke, F. *et al.* Ligand-dependent kinase activity of MERTK drives efferocytosis in human iPSC-derived macrophages. *Cell Death Dis* **12**, 538 (2021). https://doi.org:10.1038/s41419-021-03770-0

46 Scott, R. S. *et al.* Phagocytosis and clearance of apoptotic cells is mediated by MER. *Nature* **411**, 207-211 (2001). https://doi.org:10.1038/35075603

47 Seitz, H. M., Camenisch, T. D., Lemke, G., Earp, H. S. & Matsushima, G. K. Macrophages and dendritic cells use different Axl/Mertk/Tyro3 receptors in clearance of apoptotic cells. *J Immunol* **178**, 5635-5642 (2007). https://doi.org:10.4049/jimmunol.178.9.5635

48 Cohen, P. L. *et al.* Delayed apoptotic cell clearance and lupus-like autoimmunity in mice lacking the c-mer membrane tyrosine kinase. *J Exp Med* **196**, 135-140 (2002). https://doi.org:10.1084/jem.20012094

49 Belkadi, A. *et al.* Whole-exome sequencing to analyze population structure, parental inbreeding, and familial linkage. *Proc Natl Acad Sci U S A* **113**, 6713-6718 (2016). https://doi.org:10.1073/pnas.1606460113

50 Lougheed, J. C., Chen, R. H., Mak, P. & Stout, T. J. Crystal structures of the phosphorylated and unphosphorylated kinase domains of the Cdc42-associated tyrosine kinase ACK1. *J Biol Chem* **279**, 44039-44045 (2004). https://doi.org:10.1074/jbc.M406703200

51 Thakur, M. K. *et al.* Co-crystal structures of PTK6: With Dasatinib at 2.24 A, with novel imidazo[1,2-a]pyrazin-8-amine derivative inhibitor at 1.70 A resolution. *Biochem Biophys Res Commun* **482**, 1289-1295 (2017). https://doi.org:10.1016/j.bbrc.2016.12.030

52 Prieto-Echague, V., Gucwa, A., Craddock, B. P., Brown, D. A. & Miller, W. T. Cancer-associated mutations activate the nonreceptor tyrosine kinase Ack1. *J Biol Chem* **285**, 10605-10615 (2010). https://doi.org:10.1074/jbc.M109.060459

53 Tsui, T. & Miller, W. T. Cancer-Associated Mutations in Breast Tumor Kinase/PTK6 Differentially Affect Enzyme Activity and Substrate Recognition. *Biochemistry* **54**, 3173-3182 (2015). https://doi.org:10.1021/acs.biochem.5b00303

54 Kircher, M., Witten, D. M., Jain, P., O'Roak, B. J., Cooper, G. M. & Shendure, J. A general framework for estimating the relative pathogenicity of human genetic variants. *Nat Genet* **46**, 310-315 (2014). https://doi.org:10.1038/ng.2892

55 Itan, Y. *et al.* The mutation significance cutoff: gene-level thresholds for variant predictions. *Nat Methods* **13**, 109-110 (2016). https://doi.org:10.1038/nmeth.3739

56 Mahajan, K. *et al.* Ack1-mediated androgen receptor phosphorylation modulates radiation resistance in castration-resistant prostate cancer. *J Biol Chem* **287**, 22112-22122 (2012). https://doi.org:10.1074/jbc.M112.357384

57 Oelze, M., Mahmoud, K. A., Sippl, W., Wersig, T., Hilgeroth, A. & Ritter, C. A. Novel 4-anilino-alpha-carboline derivatives induce cell death in nonadhesive breast cancer cells through inhibition of Brk activity. *Int J Clin Pharmacol Ther* **53**, 1052-1055 (2015). https://doi.org:10.5414/CPXCES14EA07

58 Lachmann, N. *et al.* Large-scale hematopoietic differentiation of human induced pluripotent stem cells provides granulocytes or macrophages for cell replacement therapies. *Stem Cell Reports* **4**, 282-296 (2015). https://doi.org:10.1016/j.stemcr.2015.01.005

59 Qiu, H. & Miller, W. T. Regulation of the nonreceptor tyrosine kinase Brk by autophosphorylation and by autoinhibition. *J Biol Chem* **277**, 34634-34641 (2002). https://doi.org:10.1074/jbc.M203877200

60 Kamalati, T., Jolin, H. E., Fry, M. J. & Crompton, M. R. Expression of the BRK tyrosine kinase in mammary epithelial cells enhances the coupling of EGF signalling to PI 3-kinase and Akt, via erbB3 phosphorylation. *Oncogene* **19**, 5471-5476 (2000). https://doi.org:10.1038/sj.onc.1203931

61 Zheng, Y., Peng, M., Wang, Z., Asara, J. M. & Tyner, A. L. Protein tyrosine kinase 6 directly phosphorylates AKT and promotes AKT activation in response to epidermal growth factor. *Mol Cell Biol* **30**, 4280-4292 (2010). https://doi.org:10.1128/MCB.00024-10

62 Mahajan, K. *et al.* Ack1 mediated AKT/PKB tyrosine 176 phosphorylation regulates its activation. *Plos One* **5**, e9646 (2010). https://doi.org:10.1371/journal.pone.0009646

63 Liu, L., Gao, Y., Qiu, H., Miller, W. T., Poli, V. & Reich, N. C. Identification of STAT3 as a specific substrate of breast tumor kinase. *Oncogene* **25**, 4904-4912 (2006). https://doi.org:10.1038/sj.onc.1209501

64 Mahendrarajah, N. *et al.* HSP90 is necessary for the ACK1-dependent phosphorylation of STAT1 and STAT3. *Cell Signal* **39**, 9-17 (2017). https://doi.org:10.1016/j.cellsig.2017.07.014

65 Mao, Y. & Finnemann, S. C. Regulation of phagocytosis by Rho GTPases. *Small GTPases* **6**, 89-99 (2015). https://doi.org:10.4161/21541248.2014.989785

66 van der Horst, E. H. *et al.* Metastatic properties and genomic amplification of the tyrosine kinase gene ACK1. *Proc Natl Acad Sci U S A* **102**, 15901-15906 (2005). https://doi.org:10.1073/pnas.0508014102

67 Chan, V. W., Meng, F., Soriano, P., DeFranco, A. L. & Lowell, C. A. Characterization of the B lymphocyte populations in Lyn-deficient mice and the role of Lyn in signal initiation and down-regulation. *Immunity* **7**, 69-81 (1997). https://doi.org:10.1016/s1074-7613(00)80511-7

68 Hanke, J. H. *et al.* Discovery of a novel, potent, and Src family-selective tyrosine kinase inhibitor. Study of Lck- and FynT-dependent T cell activation. *J Biol Chem* **271**, 695-701 (1996). https://doi.org:10.1074/jbc.271.2.695

69 Hibbs, M. L. *et al.* Multiple defects in the immune system of Lyn-deficient mice, culminating in autoimmune disease. *Cell* **83**, 301-311 (1995). https://doi.org:10.1016/0092-8674(95)90171-x

70 Lamagna, C., Hu, Y., DeFranco, A. L. & Lowell, C. A. B cell-specific loss of Lyn kinase leads to autoimmunity. *J Immunol* **192**, 919-928 (2014). https://doi.org:10.4049/jimmunol.1301979

71 Nishizumi, H. *et al.* Impaired proliferation of peripheral B cells and indication of autoimmune disease in lyn-deficient mice. *Immunity* **3**, 549-560 (1995). https://doi.org:10.1016/1074-7613(95)90126-4

72 Henson, P. M. & Bratton, D. L. Antiinflammatory effects of apoptotic cells. *J Clin Invest* **123**, 2773-2774 (2013). https://doi.org:10.1172/JCI69344

73 Henson, P. M. Cell Removal: Efferocytosis. *Annu Rev Cell Dev Biol* **33**, 127-144 (2017). https://doi.org:10.1146/annurev-cellbio-111315-125315

74 Nagata, S., Hanayama, R. & Kawane, K. Autoimmunity and the clearance of dead cells. *Cell* **140**, 619-630 (2010). https://doi.org:10.1016/j.cell.2010.02.014

75 Nagata, S. Apoptosis and Clearance of Apoptotic Cells. *Annu Rev Immunol* **36**, 489-517 (2018). https://doi.org:10.1146/annurev-immunol-042617-053010

76 Kimani, S. G. *et al.* Contribution of Defective PS Recognition and Efferocytosis to Chronic Inflammation and Autoimmunity. *Front Immunol* **5**, 566 (2014). https://doi.org:10.3389/fimmu.2014.00566

77 Miyanishi, M., Segawa, K. & Nagata, S. Synergistic effect of Tim4 and MFG-E8 null mutations on the development of autoimmunity. *Int Immunol* **24**, 551-559 (2012). https://doi.org:10.1093/intimm/dxs064

78 Hanayama, R. *et al.* Autoimmune disease and impaired uptake of apoptotic cells in MFG-E8-deficient mice. *Science* **304**, 1147-1150 (2004). https://doi.org:10.1126/science.1094359

79 Hanayama, R., Tanaka, M., Miwa, K., Shinohara, A., Iwamatsu, A. & Nagata, S. Identification of a factor that links apoptotic cells to phagocytes. *Nature* **417**, 182-187 (2002). https://doi.org:10.1038/417182a

80 Kawano, M. & Nagata, S. Lupus-like autoimmune disease caused by a lack of Xkr8, a caspase-dependent phospholipid scramblase. *Proc Natl Acad Sci U S A* **115**, 2132-2137 (2018). https://doi.org:10.1073/pnas.1720732115

81 Watanabe-Fukunaga, R., Brannan, C. I., Copeland, N. G., Jenkins, N. A. & Nagata, S. Lymphoproliferation disorder in mice explained by defects in Fas antigen that mediates apoptosis. *Nature* **356**, 314-317 (1992). https://doi.org:10.1038/356314a0

82 Singer, G. G., Carrera, A. C., Marshak-Rothstein, A., Martinez, C. & Abbas, A. K. Apoptosis, Fas and systemic autoimmunity: the MRL-lpr/lpr model. *Curr Opin Immunol* **6**, 913-920 (1994).

83 Baumann, I. *et al.* Impaired uptake of apoptotic cells into tingible body macrophages in germinal centers of patients with systemic lupus erythematosus. *Arthritis Rheum* **46**, 191-201 (2002). https://doi.org:10.1002/1529-0131(200201)46:1<191::AID-ART10027>3.0.CO;2-K

84 Herrmann, M., Voll, R. E., Zoller, O. M., Hagenhofer, M., Ponner, B. B. & Kalden, J. R. Impaired phagocytosis of apoptotic cell material by monocyte-derived macrophages from patients with systemic lupus erythematosus. *Arthritis Rheum* **41**, 1241-1250 (1998). https://doi.org:10.1002/1529-0131(199807)41:7<1241::AID-ART15>3.0.CO;2-H

85 Cvetanovic, M. & Ucker, D. S. Innate immune discrimination of apoptotic cells: repression of proinflammatory macrophage transcription is coupled directly to specific recognition. *J Immunol* **172**, 880-889 (2004). https://doi.org:10.4049/jimmunol.172.2.880

86 Fadok, V. A., Bratton, D. L., Konowal, A., Freed, P. W., Westcott, J. Y. & Henson, P. M. Macrophages that have ingested apoptotic cells in vitro inhibit proinflammatory cytokine production through autocrine/paracrine mechanisms involving TGF-beta, PGE2, and PAF. *J Clin Invest* **101**, 890-898 (1998). https://doi.org:10.1172/JCI1112

87 Voll, R. E., Herrmann, M., Roth, E. A., Stach, C., Kalden, J. R. & Girkontaite, I. Immunosuppressive effects of apoptotic cells. *Nature* **390**, 350-351 (1997). https://doi.org:10.1038/37022

88 Sen, P. *et al.* Apoptotic cells induce Mer tyrosine kinase-dependent blockade of NF-kappaB activation in dendritic cells. *Blood* **109**, 653-660 (2007). https://doi.org:10.1182/blood-2006-04-017368

89 Vergadi, E., Ieronymaki, E., Lyroni, K., Vaporidi, K. & Tsatsanis, C. Akt Signaling Pathway in Macrophage Activation and M1/M2 Polarization. *J Immunol* **198**, 1006-1014 (2017). https://doi.org:10.4049/jimmunol.1601515

90 Byles, V. *et al.* The TSC-mTOR pathway regulates macrophage polarization. *Nat Commun* **4**, 2834 (2013). https://doi.org:10.1038/ncomms3834

91 Liao, X. *et al.* Kruppel-like factor 4 regulates macrophage polarization. *J Clin Invest* **121**, 2736-2749 (2011). https://doi.org:10.1172/JCI45444

92 Roberts, A. W., Lee, B. L., Deguine, J., John, S., Shlomchik, M. J. & Barton, G. M. Tissue-Resident Macrophages Are Locally Programmed for Silent Clearance of Apoptotic Cells. *Immunity* **47**, 913-927 e916 (2017). https://doi.org:10.1016/j.immuni.2017.10.006

93 Matsukawa, A. *et al.* Stat3 in resident macrophages as a repressor protein of inflammatory response. *J Immunol* **175**, 3354-3359 (2005).

94 Sica, A. & Mantovani, A. Macrophage plasticity and polarization: in vivo veritas. *J Clin Invest* **122**, 787-795 (2012). https://doi.org:10.1172/JCI59643

95 Rothlin, C. V., Carrera-Silva, E. A., Bosurgi, L. & Ghosh, S. TAM receptor signaling in immune homeostasis. *Annu Rev Immunol* **33**, 355-391 (2015). https://doi.org:10.1146/annurev-immunol-032414-112103

96 Parnaik, R., Raff, M. C. & Scholes, J. Differences between the clearance of apoptotic cells by professional and non-professional phagocytes. *Curr Biol* **10**, 857-860 (2000). https://doi.org:10.1016/s0960-9822(00)00598-4

97 Nishi, C., Toda, S., Segawa, K. & Nagata, S. Tim4- and MerTK-mediated engulfment of apoptotic cells by mouse resident peritoneal macrophages. *Mol Cell Biol* **34**, 1512-1520 (2014). https://doi.org:10.1128/MCB.01394-13

98 Seo, H. *et al.* Dual-specificity phosphatase 5 acts as an anti-inflammatory regulator by inhibiting the ERK and NF-kappaB signaling pathways. *Sci Rep* **7**, 17348 (2017). https://doi.org:10.1038/s41598-017-17591-9

99 Camenisch, T. D., Koller, B. H., Earp, H. S. & Matsushima, G. K. A novel receptor tyrosine kinase, Mer, inhibits TNF-alpha production and lipopolysaccharide-induced endotoxic shock. *J Immunol* **162**, 3498-3503 (1999).

100 Elliott, M. R. & Ravichandran, K. S. Clearance of apoptotic cells: implications in health and disease. *The Journal of cell biology* **189**, 1059-1070 (2010). https://doi.org:10.1083/jcb.201004096

101 Albert, M. L., Kim, J. I. & Birge, R. B. alphavbeta5 integrin recruits the CrkII-Dock180-rac1 complex for phagocytosis of apoptotic cells. *Nat Cell Biol* **2**, 899-905 (2000). https://doi.org:10.1038/35046549

102 Miksa, M., Komura, H., Wu, R., Shah, K. G. & Wang, P. A novel method to determine the engulfment of apoptotic cells by macrophages using pHrodo succinimidyl ester. *J Immunol Methods* **342**, 71-77 (2009). https://doi.org:10.1016/j.jim.2008.11.019

103 Shiraishi, T. *et al.* Increased cytotoxicity of soluble Fas ligand by fusing isoleucine zipper motif. *Biochem Biophys Res Commun* **322**, 197-202 (2004). https://doi.org:10.1016/j.bbrc.2004.07.098

104 Lawrence, H. R. *et al.* Development of novel ACK1/TNK2 inhibitors using a fragment-based approach. *J Med Chem* **58**, 2746-2763 (2015). https://doi.org:10.1021/jm501929n

105 Tao, H. *et al.* Macrophage SR-BI mediates efferocytosis via Src/PI3K/Rac1 signaling and reduces atherosclerotic lesion necrosis. *J Lipid Res* **56**, 1449-1460 (2015). https://doi.org:10.1194/jlr.M056689

106 Li, H. & Durbin, R. Fast and accurate short read alignment with Burrows-Wheeler transform. *Bioinformatics* **25**, 1754-1760 (2009). https://doi.org:10.1093/bioinformatics/btp324

107 McKenna, A. *et al.* The Genome Analysis Toolkit: a MapReduce framework for analyzing next-generation DNA sequencing data. *Genome Res* **20**, 1297-1303 (2010). https://doi.org:10.1101/gr.107524.110

108 Li, H. *et al.* The Sequence Alignment/Map format and SAMtools. *Bioinformatics* **25**, 2078-2079 (2009). https://doi.org:10.1093/bioinformatics/btp352

109 Itan, Y. *et al.* The human gene damage index as a gene-level approach to prioritizing exome variants. *Proc Natl Acad Sci U S A* **112**, 13615-13620 (2015). https://doi.org:10.1073/pnas.1518646112

110 Maffucci, P. *et al.* Blacklisting variants common in private cohorts but not in public databases optimizes human exome analysis. *Proc Natl Acad Sci U S A* **116**, 950-959 (2019). https://doi.org:10.1073/pnas.1808403116

111 Mullaert, J. *et al.* Taking population stratification into account by local permutations in rare-variant association studies on small samples. *Genet Epidemiol* **45**, 821-829 (2021). https://doi.org:10.1002/gepi.22426

112 Prieto-Echague, V., Gucwa, A., Brown, D. A. & Miller, W. T. Regulation of Ack1 localization and activity by the amino-terminal SAM domain. *BMC Biochem* **11**, 42 (2010). https://doi.org:10.1186/1471-2091-11-42

113 Qiu, H. & Miller, W. T. Role of the Brk SH3 domain in substrate recognition. *Oncogene* **23**, 2216-2223 (2004). https://doi.org:10.1038/sj.onc.1207339

114 Patwardhan, P., Shen, Y., Goldberg, G. S. & Miller, W. T. Individual Cas phosphorylation sites are dispensable for processive phosphorylation by Src and anchorage-independent cell growth. *J Biol Chem* **281**, 20689-20697 (2006). https://doi.org:10.1074/jbc.M602311200

115 Yokoyama, N., Lougheed, J. & Miller, W. T. Phosphorylation of WASP by the Cdc42-associated kinase ACK1: dual hydroxyamino acid specificity in a tyrosine kinase. *J Biol Chem* **280**, 42219-42226 (2005). https://doi.org:10.1074/jbc.M506996200

116 Songyang, Z. *et al.* Catalytic specificity of protein-tyrosine kinases is critical for selective signalling. *Nature* **373**, 536-539 (1995). https://doi.org:10.1038/373536a0

117 Brugnera, E. *et al.* Unconventional Rac-GEF activity is mediated through the Dock180-ELMO complex. *Nat Cell Biol* **4**, 574-582 (2002). https://doi.org:10.1038/ncb824

118 Galatro, T. F. *et al.* Transcriptomic analysis of purified human cortical microglia reveals age-associated changes. *Nat Neurosci* **20**, 1162-1171 (2017). https://doi.org:10.1038/nn.4597

119 Gosselin, D. *et al.* An environment-dependent transcriptional network specifies human microglia identity. *Science* **356** (2017). https://doi.org:10.1126/science.aal3222

120 Martin, J. C. *et al.* Single-Cell Analysis of Crohn's Disease Lesions Identifies a Pathogenic Cellular Module Associated with Resistance to Anti-TNF Therapy. *Cell* **178**, 1493-1508 e1420 (2019). https://doi.org:10.1016/j.cell.2019.08.008

121 Yang, W., Mills, J. A., Sullivan, S., Liu, Y., French, D. L. & Gadue, P. in *StemBook* (2008).

122 Toda, S., Hanayama, R. & Nagata, S. Two-step engulfment of apoptotic cells. *Mol Cell Biol* **32**, 118-125 (2012). https://doi.org:10.1128/MCB.05993-11

123 Abeyweera, T. P., Merino, E. & Huse, M. Inhibitory signaling blocks activating receptor clustering and induces cytoskeletal retraction in natural killer cells. *J Cell Biol* **192**, 675-690 (2011). https://doi.org:10.1083/jcb.201009135

124 Le Floc'h, A. *et al.* Annular PIP3 accumulation controls actin architecture and modulates cytotoxicity at the immunological synapse. *J Exp Med* **210**, 2721-2737 (2013). https://doi.org:10.1084/jem.20131324

125 Dobin, A. *et al.* STAR: ultrafast universal RNA-seq aligner. *Bioinformatics* **29**, 15-21 (2013). https://doi.org:10.1093/bioinformatics/bts635

126 Engstrom, P. G. *et al.* Systematic evaluation of spliced alignment programs for RNA-seq data. *Nat Methods* **10**, 1185-1191 (2013). https://doi.org:10.1038/nmeth.2722

127 Subramanian, A. *et al.* Gene set enrichment analysis: a knowledge-based approach for interpreting genome-wide expression profiles. *Proc Natl Acad Sci U S A* **102**, 15545-15550 (2005). https://doi.org:10.1073/pnas.0506580102

128 Liberzon, A., Subramanian, A., Pinchback, R., Thorvaldsdottir, H., Tamayo, P. & Mesirov, J. P. Molecular signatures database (MSigDB) 3.0. *Bioinformatics* **27**, 1739-1740 (2011). https://doi.org:10.1093/bioinformatics/btr260

FIGURES

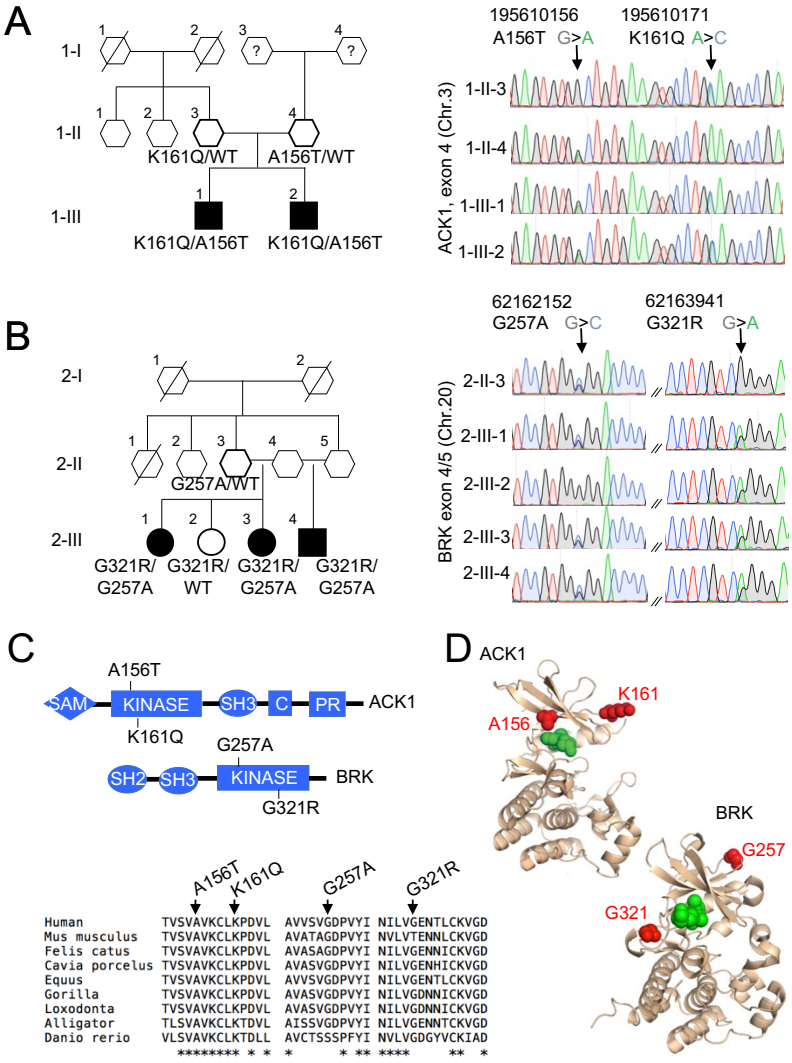

Figure 1. NRTK compound heterozygous missense variants in two multiplex families with SLE. (**A, B**) **Pedigrees and Sanger re-sequencing** of DNA from patients and healthy relatives of kindred 1 (A) carrying K161Q and A156T ACK1 mutations and kindred 2 (B) carrying G257A and G321R BRK mutations. Individuals with SLE are indicated by black boxes; deceased individuals are shown by diagonal bar; bold indicates the members analyzed by WES; squares indicate males, circles indicate females, and hexagons indicate generation I or II individuals with undisclosed sex for confidentiality. Black: Guanine, green: Adenine, red: Thymidine, blue: Cytosine. Arrows indicate nucleotide substitutions. Text indicates amino-acid substitutions. **(C) Domain architecture** (top panel) of ACK1 and BRK, with indicated mutations. SH2, Src homology 2; SH3, Src homology 3; Kinase, tyrosine kinase domain; C, Cdc42 binding domain; PR, Proline rich domain; SAM, Sterile α motif. **Alignment of kinase domains** (bottom panel) from ACK1 and BRK orthologs. Arrows indicate positions of mutations and stars indicate the amino acids conserved throughout species. **(D) Three dimensional (3D) structures of ACK1 and BRK.** *Top*: the crystal structure of ACK1 in a complex with AMP-PCP (PDB ID: 1U54). The mutated residues (A156 and K161) are shown in red, and the nucleotide analog is in green. *Bottom*: the crystal structure of BRK in a complex with the ATP-competitive inhibitor dasatinib (PDB ID: 5H2U). The mutated residues (G257 and G321) are shown in red, and dasatinib is in green.

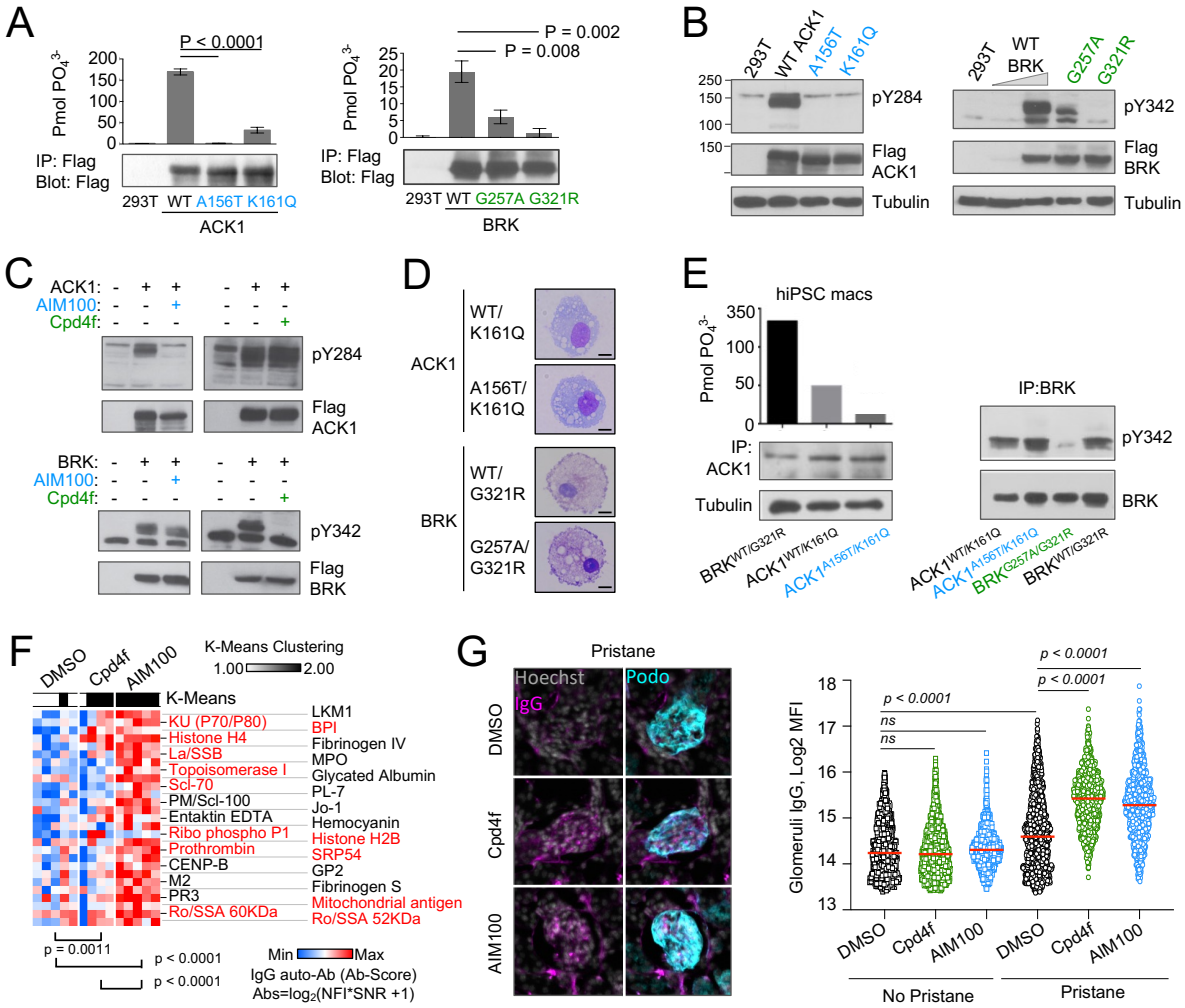

Figure 2. ACK1 and BRK mutations are null and hypomorph alleles and their blockade exacerbates pristane induced SLE in Balb/c mice. (A) Immunoprecipitation (IP) kinase assay. ACK1 *(Top)* was immunoprecipitated from 293T cells expressing Flag-tagged ACK1 wild type (WT), ACK1 A156T, or ACK1 K161Q with anti-Flag Ab. Immunoprecipitated proteins were used for duplicate in vitro kinase reactions with WASP synthetic peptide. Samples of the immunoprecipitates were also probed with anti-Flag Ab. BRK *(bottom)* was immunoprecipitated as above from 293T cells expressing Flag-tagged BRK WT and mutants with anti-Flag Ab. Kinase reactions were performed with peptide AEEEIYGEFEAKKKG, and represented as above, and samples of the immunoprecipitates probed with anti-Flag Ab. p-values were calculated using an *Anova* test (Tukey's multiple comparisons test). **(B) Western blot analyses** of lysates from 293T cells expressing (left panel) Flag-tagged WT or mutant forms ACK1 probed with anti-ACK1 Tyr(P)^{284} (PY284), anti-Flag and anti-tubulin antibodies (Ab), and expressing (right panel) Flag-tagged WT or mutant BRK probed with anti-BRK Tyr(P)^{342} (PY342), anti-Flag and anti-tubulin antibodies. For BRK, 293T cells were starved overnight, and stimulated with 100 ng/ml EGF for 10 min. The lysate from WT BRK indicated as low was from cells transfected with one-tenth the amount of WT DNA. **(C)** Western blot analyses of lysates from 293T cells expressing ACK1-Flag or BRK-Flag treated with AIM100 or Cpd4f and probed with anti-ACK1 Tyr(P)284 (PY284) or anti-BRK Tyr(P)342 (PY342) and anti-Flag antibodies. **(D)** May-Grunwald-Giemsa staining of iPSC-derived macrophages from familial controls and ACK1 and BRK patients. Scale bar 10 µm, 100X

objective. Representative images from over 50 observed cells per line. **(E) Immunoprecipitation (IP) kinase assay in patients' macrophages.** (Left panel) ACK1 was immunoprecipitated from BRK$^{WT/G321R}$, ACK1$^{WT/K161Q}$ and ACK1$^{A156T/K161Q}$ iPSCs-derived macrophages with anti-ACK1 Ab. The immunoprecipitated proteins were used in duplicate for in vitro kinase reactions with WASP synthetic peptide. Samples of the immunoprecipitates were also probed with anti-ACK1 Ab and anti-tubulin Ab. (Right panel) BRK was immunoprecipitated from ACK1$^{WT/K161Q}$, ACK1$^{A156T/K161Q}$, BRK$^{WT/G321R}$ and BRK$^{G257A/G321R}$ iPSCs-derived macrophages with anti-BRK Ab. The immunoprecipitated proteins were probed with anti-BRK Tyr(P)^{342} (PY342) and anti-BRK antibodies. **(F) Heat map of IgG auto-antibodies detected in serum of mice treated with inhibitors.** Heatmaps show autoantigen microarray panel performed on serum from 4 month-old BALB/cByJ female mice which received a weekly intra-peritoneal injection of DMSO (vehicle, 20ul/mice), AIM100 (25mg/kg in 20ul), or Cpd4f (20mg/kg in 20ul/) since the age of five weeks, and Pristane injection at 5 week of age. Plotted values represent Ab Scores (Log_2 [antigen net fluorescence intensity (NFI) x signal to noise ratio (SNR) +1]. Heatmap columns represent serum analysis of independent mice (n=4-5 for each of the 3 conditions). Heatmap rows sorted top to bottom starting with most significantly increased Ab Score in Cpd4f and AIM100 mice in comparison to DMSO treated mice. Single row p-value between DMSO/Cpd4f and DMSO/AIM100 treated mice were calculated by a paired t-test. Full panel p-values were calculated using a paired t-test. Hierarchical clustering is based on one minus Pearson correlation with complete linkage method. K-means clustering is based on Euclidean distance, with 2 clusters, with 10000 maximum iterations. **(G) Immunofluorescence for mouse IgG on kidney sections.** Representative micrographs (left) displaying glomeruli on kidney sections from 4 month-old BALB/cByJ female mice treated as in (F) and stained with Hoechst 33342, anti-mouse IgG, and anti-mouse Podoplanin antibody. In the quantification plot (right panel) each symbol represents the IgG mean fluorescence intensity (MFI) in a single glomerulus, of mice treated with designated inhibitors, in the presence or absence of pristane. Approximately 250 glomeruli we analyzed per section/mouse (>95% of all glomeruli in an entire longitudinal kidney section). n≥4 mice. P-values were obtained using an Anova test with Tukey's correction for multiple comparisons.

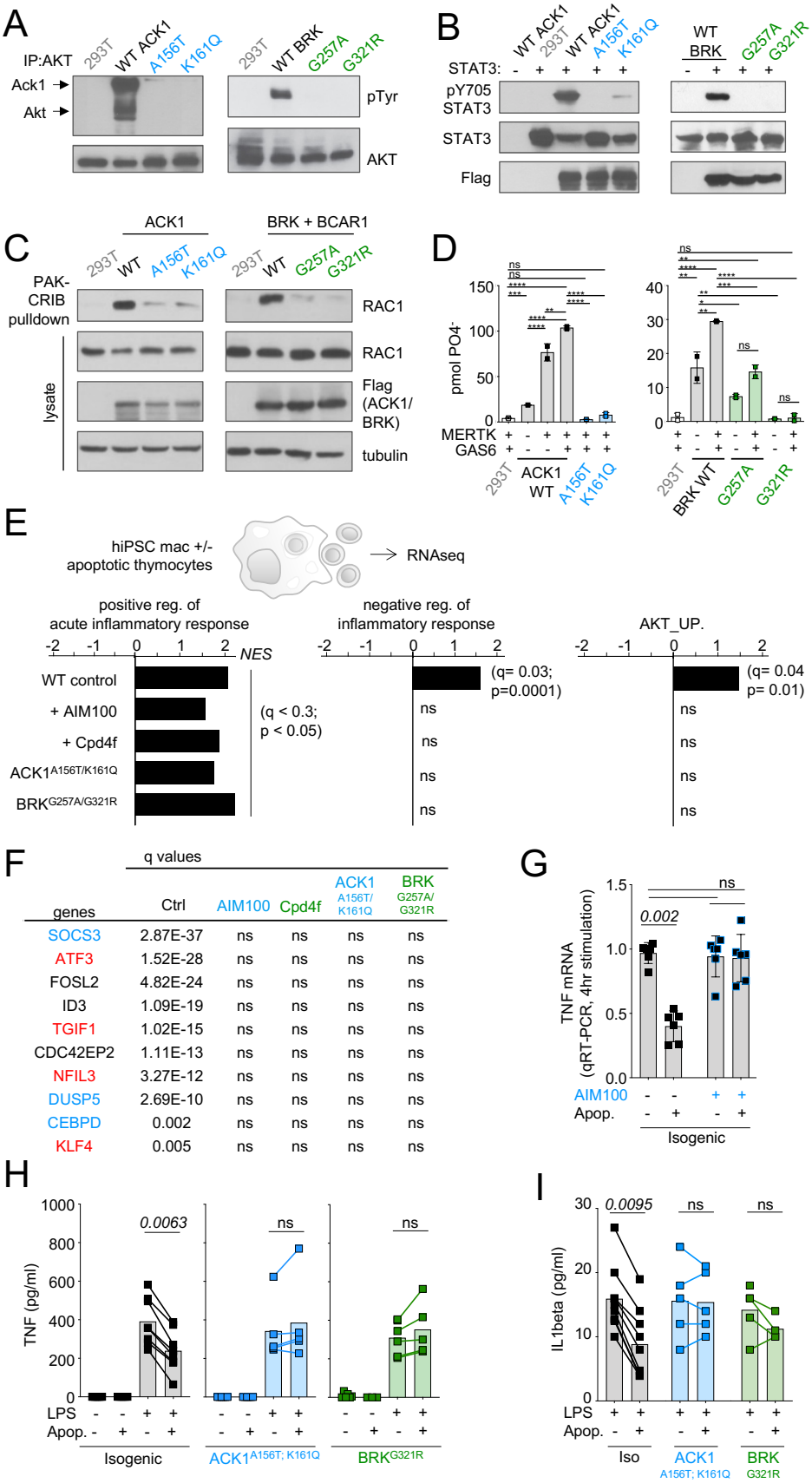

Figure 3. ACK1 and BRK kinase deficiency disrupts the anti-inflammatory response driven by apoptotic cells in macrophages. (A) Western blot analysis for AKT phosphorylation by

ACK1 and BRK. Cell lysates from 293T cells were incubated with anti-AKT. Immunoprecipitated proteins were probed with anti-phosphotyrosine and anti-AKT antibodies. **(B) Western blot analysis for STAT3 phosphorylation by ACK1 and BRK**. Lysates from 293T cells coexpressing STAT3 and Flag-tagged WT or mutant forms (A156T and K161Q) of ACK1 or mutant forms (G257A and G321R) of BRK were probed with anti-phospho-STAT3 (Tyr705), anti-STAT3 and anti-Flag antibodies. For analysis of BRK, cells were treated with 100 ng/ml EGF for 10 min. **(C) RAC activation by WT ACK1 and BRK.** Cell lysates from 293T cells expressing WT or mutant forms of ACK1 (*left*) and lysates from 293T cells expressing WT or mutant forms of BRK (*right*) were incubated with GST-PAK CRIB sepharose beads, and the level of RAC1 GTP was determined by immunoblotting with anti-Rac1 antibody. Lysates were also probed with anti-Rac1, anti-FLAG and anti-tubulin antibody. For analysis of BRK, 293T cells were cotransfected with CAS and stimulated with 100 ng/ml EGF for 10 min. (**D) MERTK increases kinase activity of BRK and ACK1.** IP kinase assay. ACK1 (left) was immunoprecipitated from 293T cells co-transfected with Flag-tagged ACK1 WT, ACK1 A156T, or ACK1 K161Q and MERTK with anti-Flag Ab. Immunoprecipitated proteins were used in duplicate in vitro for kinase reactions with WASP synthetic peptide and results represented as pmol phosphate transferred. BRK (right) was immunoprecipitated as above from 293T cells co-transfected with Flag-tagged BRK WT or mutants and MERTK with anti-Flag Ab. Kinase reactions was performed with peptide AEEEIYGEFEAKKKG, and represented as above. P-values were calculated using an Anova test (Tukey's multiple comparison test) ($p > 0.05$ (ns); $p < 0.05$ (*); $p < 0.01$ (**); $p < 0.001$ (***); $p < 0.0001$ (****). **(E**) **Regulation of inflammatory response.** Significant normalized enrichment scores (NES) for GO 'positive regulation of acute inflammation' gene set, GO 'negative regulation of inflammatory response' gene set, and GO 'AKT_UP.V1_UP' gene set in WT and mutant macrophages, and WT treated with AIM100 (2 μM) or Cpd4f (0.5 μM), exposed to apoptotic cells, with 3 replicates per experimental condition. Significant enrichment (p-value<0.05 and FDR (q-value) <0.25) are calculated as reported in methods. **(F)** Table of the top 10 differentially regulated genes by apoptotic cells in WT macrophages are not differentially expressed in mutant macrophages and WT macrophages treated with AIM100 or Cpd4f (treated as in E). Numbers indicate FDR (q-value). Known target genes of STAT3 and AKT are labeled in blue and red respectively (**G**) **TNF mRNA production by** WT macrophages treated with AIM100 (2 μM) 4hrs after exposure to apoptotic cells. n=6, from 2 independent experiments. (**H,I) TNF and IL1b production by macrophages**, as measured by ELISA on media collected from mutant and isogenic WT macrophages (C12.1) incubated with mouse apoptotic thymocytes for 90 min, then stimulated with LPS (1 ng/ml) for 18 h. n≥4, from ≥2 independent experiments. P-values in G-I were calculated using an *Anova* test with Tukey's correction for multiple comparisons.

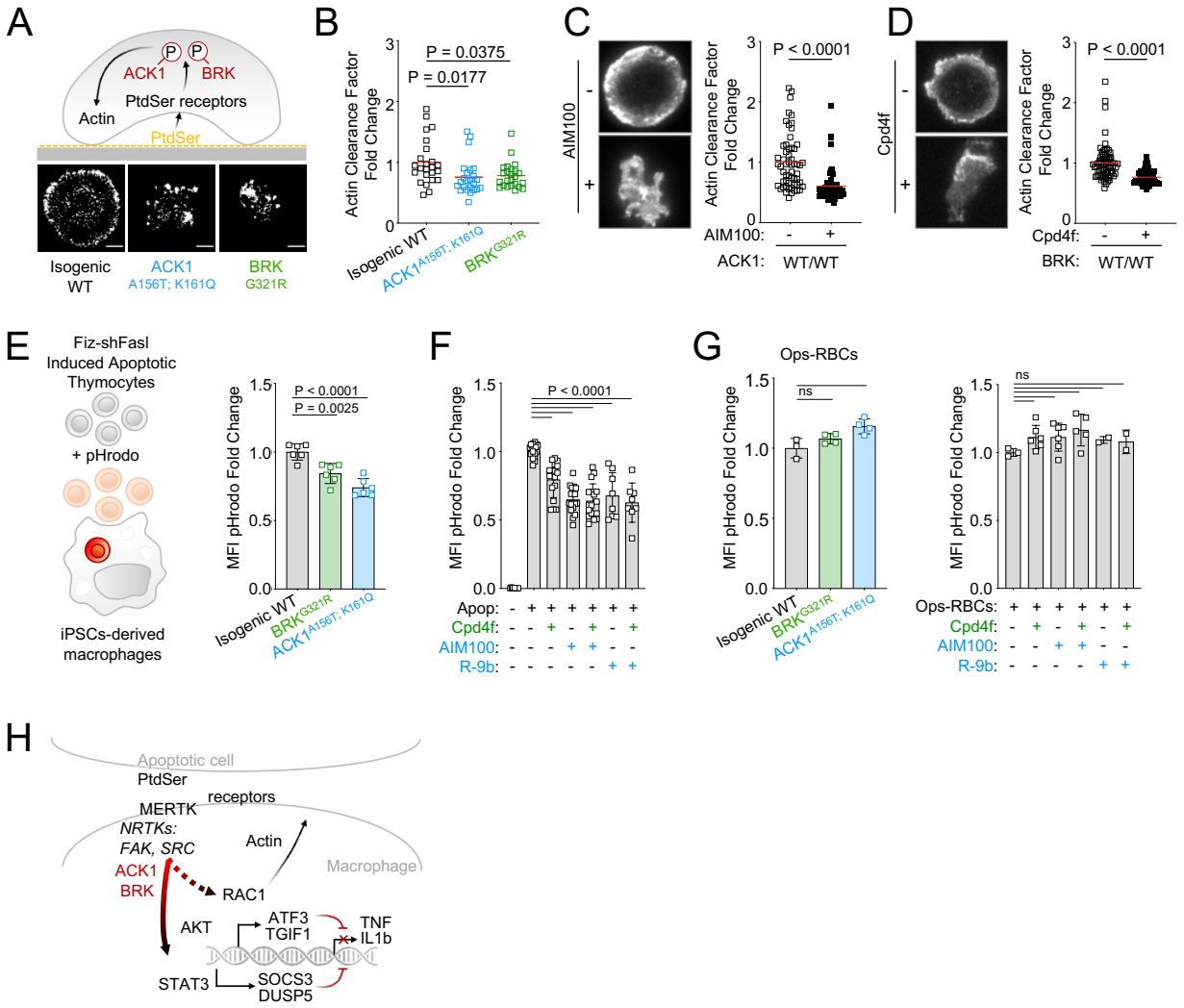

Figure 4. ACK1 and BRK kinase deficiency alter actin remodeling at the phagocytic cup and modestly decrease engulfment of apoptotic cells in macrophages. (A) Actin remodeling in macrophages. Schematic and representative images of of F-actin by TIRF microscopy in macrophages of indicated genotype, deposited on PtdSer-coated plates for 20 min. **(B)** Quantification of actin clearance factor for macrophages of the indicated genotypes. Actin remodeling (actin clearance factor) was calculated as a ratio of F-actin staining intensity at cell border divided by F-actin staining intensity at cell center. The actin clearance factor ratios were normalized to the mean value of WT control. Each replicate indicates actin clearance factor fold change from WT mean in single cells. n>20, from 2 independent experiments. Red lines denote the mean. P-values are obtained using an *Anova* test with Tukey's correction for multiple comparisons. **(C,D) Actin remodeling** quantification (as in A,B) and representative TIRF images of WT macrophages (C12.1 line) pretreated with DMSO, AIM100 (2 μM) or Cpd4f (0.5 μM). n>24, from 3 independent experiments **(E,F) Uptake of apoptotic cells. (E)** Schematic depicts uptake of apoptotic mouse thymocytes treated with Fiz-shFASL and labeled with the pH-sensitive dye pHrodo by iPSC-derived macrophages. Isogenic WT (C12.1 line) and isogenic ACK and BRK point mutant macrophages were incubated with pHrodo-labeled mouse apoptotic thymocytes for 90 minutes and analyzed by flow cytometry. Graph represents mean pHrodo fluorescence Intensity (MFI) fold change calculated by dividing total pHrodo MFI (610/20 nm) of individual

samples by the average MFI of isogenic WT macrophages. n≥3, from 3 independent experiments. P-values were obtained using an *Anova* test with Tukey's correction for multiple comparisons. (**F)** Uptake of apoptotic cells as in (E) with WT macrophages (C12.1 line) pretreated with AIM100 (2 µM), R-9b (4 µM), Cpd4f (0.5 µM), or DMSO. n≥8, from ≥4 independent experiments. **(G) Uptake of opsonized sheep red blood cells.** WT macrophages (C12.1 line) are pretreated as in (F) and incubated with opsonized pHrodo sheep red blood cells for 90 min. Graphs represent mean fluorescence Intensity (MFI) fold change calculated by dividing total pHrodo MFI (610/20 nm) of individual samples by the average MFI of WT macrophages. n≥2, from 2 independent experiments. P-values are obtained using an *Anova* test with Tukey's correction for multiple comparisons. (**H)** Schematic representation of ACK1 and BRK proposed function in efferocytosis.

FIGURE SUPPLEMENTS

A

chr	position	allele	rs	impact	gene	AAchange	COL0254 (patient III1)	COL0255 (patient III2)	COL0257 (father II4)	COL0256 (mother II3)	HZ-inhouse	HO-inhouse	MAF (gnomAD)	CADD/MSC	GDI
X-linked															
X	32328278	T/C	rs764943244	missense	DMD (Dystrophin)	E2009G	ho(0/6)	ho(0/9)		he(8/7)	0	0	All 10-5 S. Asia 10-4	high (26/0.002)	18.86
X	153218211	C/T	rs368279501	missense	HCFC1 (Host Cell Factor C1)	V1566M	ho(0/11)	ho(0/19)		he(12/21)	1	0	All 2 10-4 Africa 1.7 10-3	low (12/25)	1.74
Homozygous															
9	115095104	G/A	rs528795752	missense	PTBP3 (Polypyrimidine Tract Binding Protein 3)	P7L	ho(0/14)	ho(0/17)	he(7/5)	he(10/8)	20	0	All 0.0056 S. Asia 0.039	low (1.2/3.3)	1.42
Compound heterozygous															
3	195610156	T/G		missense	ACK1/TNK2 (Tyrosine Kinase Non Receptor 2)	K161Q	he(4/10)	he(14/6)		he(9/18)	0	0	0	high (24/2.3)	5.4
3	195610171	C/T		missense		A156T	he(10/3)	he(5/9)	he(9/8)		0	0	0	high (34/2.3)	
19	9015724	G/A	rs140100296	missense	MUC16 (Mucin 16)	P12700L	he(3/4)	he(6/5)		he(5/7)	0	0	0	high (8.5/3.3)	31.77
19	9067884	G/T	rs371540601	missense		T6521N	he(18/8)	he(16/7)	he(13/10)		3	0	All 7.6 10-5 Europe 1.3 10-4	low (0.01/3.3)	

B

chr	position	allele	rs	impact	gene	AAchange	COL0602 (healthy sister III2)	COL0603 (healthy mother	COL0600 (patient III4)	COL0601 (patient III1)	COL0599 (patient III3)	HZ-inhouse	HO-inhouse	MAF (gnomAD)	CADD/MSC	GDI
Compound heterozygous																
3	57415434	T/G	rs145799134	missense	DNAH12 (Dynein Axonemal Heavy Chain 12)	D1683A			he(43/57)	he(37/41)	he(44/37)	30	2	All 0.009 Europe 0.029	high (31/2.3)	18.49 high
3	57443467	A/T	rs151214809	missense		V1106E	he(15/12)	he(26/32)	he(28/30)	he(21/21)	he(14/20)	30	4	All 0.003 Africa 0.015	high (23.5/2.3)	
20	62162152	C/T	rs146772563	missnse	BRK/PTK6 (Protein Tyrosine Kinase 6)	G321R		he(51/26)	he(39/44)	he(29/32)	he(23/20)	1	0	All 0.000173 Africa 0.001	high (26.7/2.3)	2 medium
20	62163941	C/G		missense		G257A	he(15/12)		he(25/16)	he(22/11)	he(20/11)	0	0	All 8 10-6 Africa 8 10-5	high (21.6/2.3)	
5	66461583	C/T	rs56201012	missense	MAST4 (Microtubule Associated Ser/Thr Kinase Family Menber 4)	H1249Y		he(25/31)	he(32/23)	he(15/19)	he(33/27)	53	3	All 0.007 Africa 0.09	high (7/2.3)	6.2 medium
5	66461974	G/A	rs200784710	missense		V2323I	he(26/38)		he(27/22)	he(16/27)	he(59/63)	0	0	All 0.0002 Africa 0.0028	high (14/2.3)	

C

Name	transcript ID	RefSeq	Protein	position of our variants
TNK2-201	ENST00000333602.11	NM_005781	1038aa	A156T; K161Q
TNK2-208	ENST00000428187.5	NM_00138046	1040aa	A188T; K193Q
TNK2-202	ENST00000381916.6	NM_001010938	1086aa	A219T; K224Q

D

Ethnic subgroup			Number of alleles	Closest ethnic origin with described individuals from 1kG	Kindred 1				Kindred 2			
					A156T in TNK2 [ACK1] (MAF)		K161Q in TNK2 [ACK1] (MAF)		G321R in PTK6 [BRK] (MAF)		G257A in PTK6 [BRK] (MAF)	
					1kG	gnomAD	1kG	gnomAD	1kG	gnomAD	1kG	gnomAD
AFR	LWK	Luhya in Webuye, Kenya	198	2.III.1, 2.III.2, 2.III.3	0		0		0		0	
AFR	ACB	African Caribbean in Barbados	192	2.III.1, 2.III.2, 2.III.3	0		0		0.005		0	
AFR	GWD	Gambian in Western Division, The Gambia - Mandinka	226		0		0		0.004		0	
AFR	ASW	African Ancestry in Southwest US	122	2.III.1, 2.III.2, 2.III.3	0	0	0	0	0	0.00136	0	8E-05
AFR	MSL	Mende in Sierra Leone	170		0		0		0.006		0	
AFR	ESN	Esan in Nigeria	198		0		0		0.005		0	
AFR	YRI	Yoruba in Ibadan, Nigeria	216		0		0		0		0	
AMR	MXL	Mexican Ancestry in Los Angeles, California	128		0		0		0		0	
AMR	PEL	Peruvian in Lima, Peru	170		0	0	0	0	0	0.0002	0	0
AMR	CLM	Colombian in Medellin, Colombia	188		0		0		0		0	
AMR	PUR	Puerto Rican in Puerto Rico	208		0		0		0		0	
EAS	CHD	Chinese in Denver, Colorado	0		0		0		0		0	
EAS	JPT	Japanese in Tokyo, Japan	208		0		0		0		0	
EAS	CDX	Chinese Dai in Xishuangbanna, China	186		0	0	0	0	0	0	0	0
EAS	CHB	Han Chinese in Beijing, China	206		0		0		0		0	
EAS	KHV	Kinh in Ho Chi Minh City, Vietnam	198		0		0		0		0	
EAS	CHS	Han Chinese South	210		0		0		0		0	
EUR	FIN	Finnish in Finland	198		0	0	0	0	0	0	0	0
EUR	GBR	British in England and Scotland	182		0		0		0		0	
EUR	TSI	Toscani in Italy	214		0	0	0	0	0	1.6E-05	0	0
EUR	IBS	Iberian populations in Spain	214		0		0		0		0	
EUR	CEU	Utah residents (CEPH) with North and West European ancestry	198		0		0		0		0	
SAS	ITU	Indian Telugu in the UK	204		0		0		0		0	
SAS	STU	Sri Lankan Tamil in the UK	204		0		0		0		0	
SAS	GIH	Gujarati Indian in Houston, TX	206	1.III.1, 1.III.2	0	0	0	0	0	0	0	0
SAS	BEB	Bengali in Bangladesh	172	1.III.1, 1.III.2	0		0		0		0	
SAS	PJL	Punjabi in Lahore, Pakistan	192	1.III.1, 1.III.2	0		0		0		0	

Figure 1-figure supplement 1. Candidate genes identified by WES analysis in family 1 and family 2. (A) Candidate genes identified in family 1. For a complete penetrance, 3 models of inheritance were applied: homozygous, X-linked, and compound heterozygous. Non-synonymous

coding mutation with MAF< 0.01 were selected and reported for each model of inheritance. The red box shows the ACK1 mutants identified. Total MAF and maximal MAF are reported. Amino acid positions are based on transcript ENST00000333602.11. **(B) Candidate genes identified in family 2**. For a complete penetrance, 2 models of inheritance were applied: homozygous and compound heterozygous. Non-synonymous coding mutation with MAF<0.01 were selected and reported for each model of inheritance. The red box shows the PTK6 mutants identified. Total MAF and maximal MAF are reported. Amino acid positions are based on transcript ENST00000542869.2. **(C) ACK1 transcripts** with NM number reported in Ensembl. ACK1 mutant positions in the respective transcripts are reported. **(D) ACK1 and BRK mutant alleles frequency across different ethnic subgroups.** Analysis of 27 GWAS studies of SLE (https://www.gwascentral.org/) found no common variants in the close vicinity of the ACK1 (TNK2) or BRK (PTK6) genes with a p-value lower than 5.10-8, the threshold of significance for GWAS.

position	ref	alt	Patient 2-III-1		Patient 2-III-3		Patient 2-III-4		Healthy sister 2-III-2		Healthy mother 2-II-3		Father deduced 2-II-4		function	AAChange
62159762	T	A									A	A			downstream	0
62160481	C	A	C	A	C	A	C	A	A	A	C	A		A	utr_3	0
62160709	G	A	G	A	G	A	G	A	A	A	G	A		A	utr_3	0
62161418	G	C	C	C	C	C	C	C	C	C	C	C		C	intron	0
62161421	G	A	G	A	G	A	G	A	A	A	G	A		A	intron	0
62161422	G	A	G	A	G	A	G	A	G	G	G	A		G	intron	0
62161649	C	T	C	C	C	C	C	C	C	T	C	T		C	intron	0
62161713	C	T	C	T	C	T	C	T	C	C	C	T		C	intron	0
62162058	G	A	G	A	G	A	G	A	G	G	G	A		G	intron	0
62162152	C	T	C	**T**	C	**T**	C	**T**	C	**T**	C	C	?	**T**	missense	p.Gly321Arg
62162340	T	C	C	C	C	C	C	C	C	C	C	C		C	intron	0
62163680	CTGT	C													intron	0
62163693	TGTGTGC	T													intron	0
62163704	G	C													intron	0
62163707	T	A													intron	0
62163708	C	G													intron	0
62163740	GTGTC	G													intron	0
62163793	T	C	C	C	C	C	C	C	C	C	C	C		C	intron	0
62163803	TGGG	T	T	T	T	T	T	T	T	T	T	T		T	intron	0
62163941	C	G	C	**G**	C	**G**	C	**G**	C	C	C	**G**		C	missense	p.Gly257Ala
62164169	GC	G	G	G	G	G	G	G	G	G	G	G		G	intron	0
62164193	C	T	T	T	T	T	T	T	T	T	T	T		T	intron	0
62164242	G	A													intron	0
62164263	G	A													intron	0
62164713	C	A													intron	0
62164714	C	T													intron	0
62164787	G	A	A	A	A	A	A	A	A	A	A	A		A	intron	0
62164790	T	C	C	C	C	C	C	C	C	C	C	C		C	intron	0
62164795	G	A	A	A	A	A	A	A	A	A	A	A		A	intron	0
62164809	T	G	G	G	G	G	G	G	G	G	G	G		G	intron	0
62165034	A	G	G	G	G	G	G	G	G	G	G	G		G	synonymous	p.His180His
62165065	A	G	G	G	G	G	G	G	G	G	G	G		G	splicing	0
62165086	G	A	G	A	G	A	G	A	G	G	G	A		G	intron	0
62165135	G	A	A	A	A	A	A	A	A	A	A	A		A	intron	0
62165202	G	C	C	C	C	C	C	C	C	C	C	C		C	intron	0
62165803	GC	G	G	G	G	G	G	G	G	G	G	G		G	intron	0
62165821	C	T	T	T	T	T	T	T	T	T	T	T		T	intron	0
62166226	G	A	G	G	G	A	G	A	G	G	G	A		G	intron	0
62166573	C	G	C	C	C	C	C	C	C	C	C	C		C	intron	0
62168234	G	A	G	G	G	G	G	G	G	G	G	G		G	intron	0

Figure 1-figure supplement 2. **Haplotype member's family 2**. SNPs close to the G321R mutation are reported for the 3 patients, the healthy sister, the healthy mother and deduced for the healthy father.

A

Gene	Protein	Chrom	inheritance pattern	ref.
C1q	C1q	1	AR	*Pickering et al; Botto et al*
C1r/s	C1r/s	12	AR	
C4	C4	6	AR	
C2	C2	6	AR	
C3	C3	19	AR	
TREX1	TREX1	3	AR/AD	*Rice et al; Lee-Kirsch et al*
DNase1	DNase1	16	AD	*Yasutomo et al*
DNase1L3	DNase1L3	3	AR	*Al-Mayouf et al*
CYBB	gp91phox	X	X-linked	*Xie et al*
CYBA	p22phox	16	AR	
NCF2	p67phox	1	AR	
NCF1	p47phox	7	AR	
NCF4	p40phox	22	AR	

Gene	Protein	Chrom	inheritance pattern	ref.
SHOC2	SHOC2	10	AD	*Bader-Meunier et al*
KRAS	KRAS	12	AD	
PTPN11	PTPN11	12	AD	
TMEM173	STING	5	AD	*Jeremiah et al*
IFIH1	MDA5	2	AD	*Crow et al*
ADAR1	ADAR1	1	AR	
SAMHD1	SAMHD1	20	AR	
ACP5	TRAP	19	AR	*Briggs et al*
STAT1	STAT1	2	AD	*Toubiana et al*
PRKCD	PKCδ	3	AR	*Belot et al; Kiykim et al; Salzer et al*

B

Patient	Chr	ID	fuction	gene	AAChange	zygo	ExAC_Freq	CADD	MSC	MSC_99%	GDI	inheritance pattern
Family 5 III 2	1	rs35937854	missense	NCF2	p.Val297Ala	het	0.0037	22.9	0.09	HIGH	13.43	AR
Family 5 III 4	1	rs35937854	missense	NCF2	p.Val297Ala	het	0.0037	22.9	0.09	HIGH	13.43	AR
Family 10 III 2	1	rs17843865	missense	ADAR	p.Tyr587Cys	het	0.0042	0.238	0.5	LOW	1.88	AR
Family 10 IV 5	1	rs17843865	missense	ADAR	p.Tyr587Cys	het	0.0042	0.24	0.5	LOW	1.88	AR

Patient	Chr	ID	fuction	gene	AAChange	zygo	ExAC_Freq	CADD	MSC	MSC_99%	GDI	inheritance pattern	Splicing prediction Human Splicing Finder
Family 3 III 1	2	rs143870870	synonymous	IFIH1	p.Thr86Thr	het	0.0016	6.436	19.33	LOW	13.41	AD	no
Family 3 III 7	2	rs143870870	synonymous	IFIH1	p.Thr86Thr	het	0.0016	6.436	19.33	LOW	13.41	AD	no
Family 5 III 2	19	rs34375794	synonymous	ACP5	p.Asp92Asp	het	0.0015	10.05	4.58	HIGH	5.82	AR	no
Family 5 III 4	19	rs34375794	synonymous	ACP5	p.Asp92Asp	het	0.0015	10.05	4.58	HIGH	5.82	AR	no
Family 7 III 4	19	rs77911902	synonymous	ACP5	p.Thr285Thr	het	0.01	1.55	4.58	LOW	5.82	AR	no
Family 7 III 11	19	rs77911902	synonymous	ACP5	p.Thr285Thr	het	0.01	1.55	4.58	LOW	5.82	AR	no
Family 7 III 4	3	rs56338517	synonymous	PRKCD	p.Ala642Ala	het	0.0094	12.62	26.5	LOW	1.14	AR	no
Family 7 III 11	3	rs56338517	synonymous	PRKCD	p.Ala642Ala	het	0.0094	12.62	26.5	LOW	1.14	AR	no

Figure 1-figure supplement 3. **SLE-causing genes**. **(A)** List of genes already described as disease-causing gene in Lupus. **(B)** Synonymous and non-synonymous mutations with a MAF<0.01 in the coding region of known SLE-causing genes identified in the 10 kindreds. Only mutations segregating with disease in the kindreds were selected.

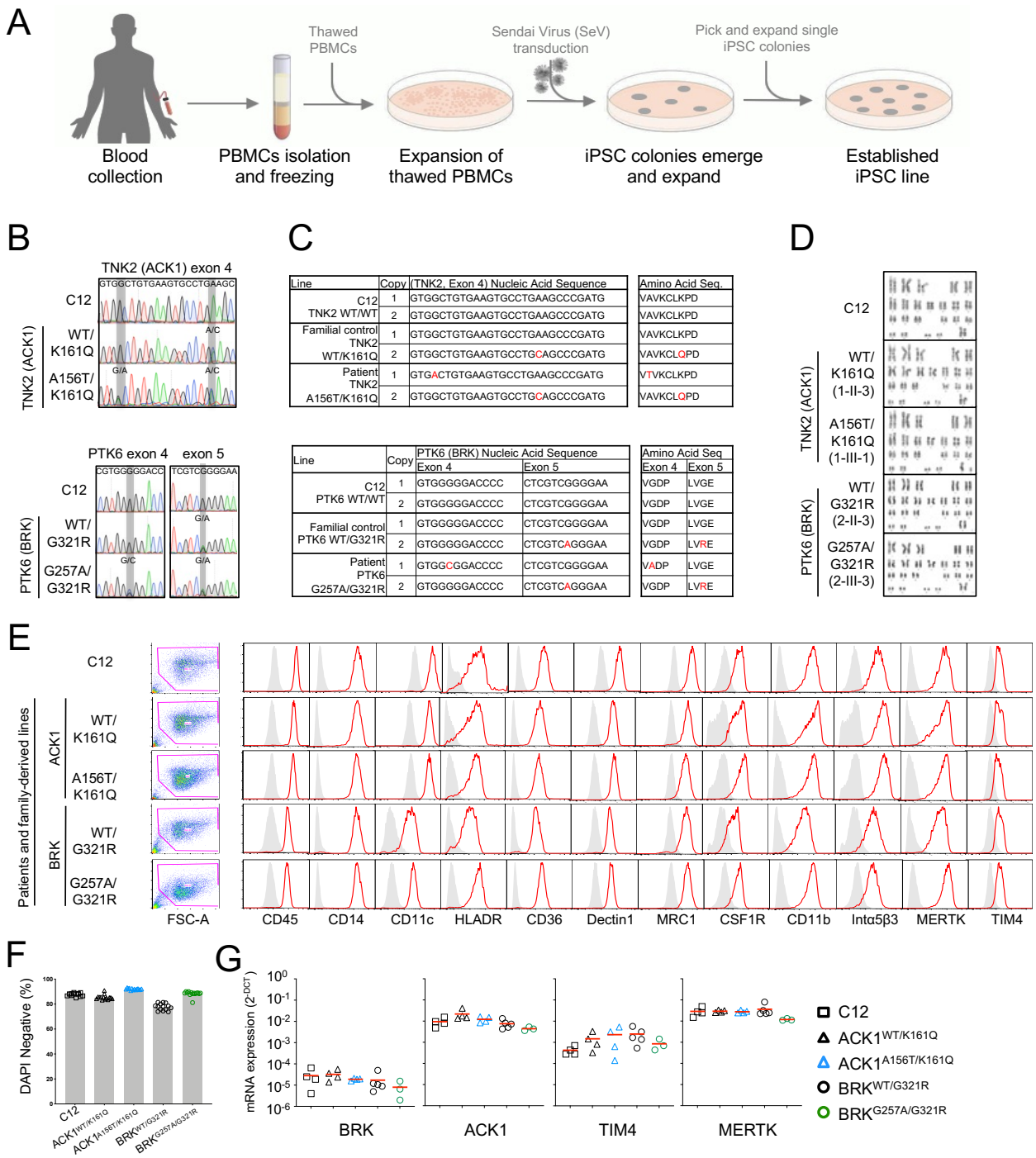

Figure 2-figure supplement 1. Generation and characterization of control and patient derived iPSCs and iPSC-macrophages. (A) Schematic representation of the process of reprograming peripheral blood mononuclear cells (PBMCs) into induced pluripotent stem cells (iPSCs). See methods for details. **(B)** Sanger sequencing of reprogrammed iPSC lines from unrelated wild type (WT) control (C12), familial controls (1-II-3 $ACK1^{WT/K161Q}$ and 2-II-3 $BRK^{WT/G321R}$), and SLE patients (1-III-1 $ACK1^{A156T/K161Q}$ and 2-III-3 $BRK^{G257A/G321R}$). Gray bars indicate positions of nucleotide substitution. **(C)** Nucleic acid and predicted amino acid sequences for both gene copies of TNK2(AKC1) or PTK6(BRK) in iPSC lines from C12 and SLE families. Variations from WT are indicated in red. **(D)** Karyotypes of iPSC lines from C12 and SLE families. Chromosome analysis was performed on a minimum of 20 DAPI-banded metaphases. **(E) Flow**

cytometry analysis of surface receptor expression on iPSC derived macrophages from C12, familial controls, and SLE patients iPSC lines. Histograms show fluorescence intensity for indicated antibodies (red) and FMO controls (grey). **(F)** Bar plots show percent viability based on DAPI staining of macrophages derived from C12, familial controls, and SLE patients iPSC lines. **(G) RT-QPCR analysis of mRNA for** BRK, ACK1, TIM4, and MERTK. mRNA expression was normalized to GAPDH ($2^{-\Delta Ct}$) (see methods). n≥2, from 1-2 independent experiments. P-values were obtained using an Anova test with Tukey's correction for multiple comparisons.

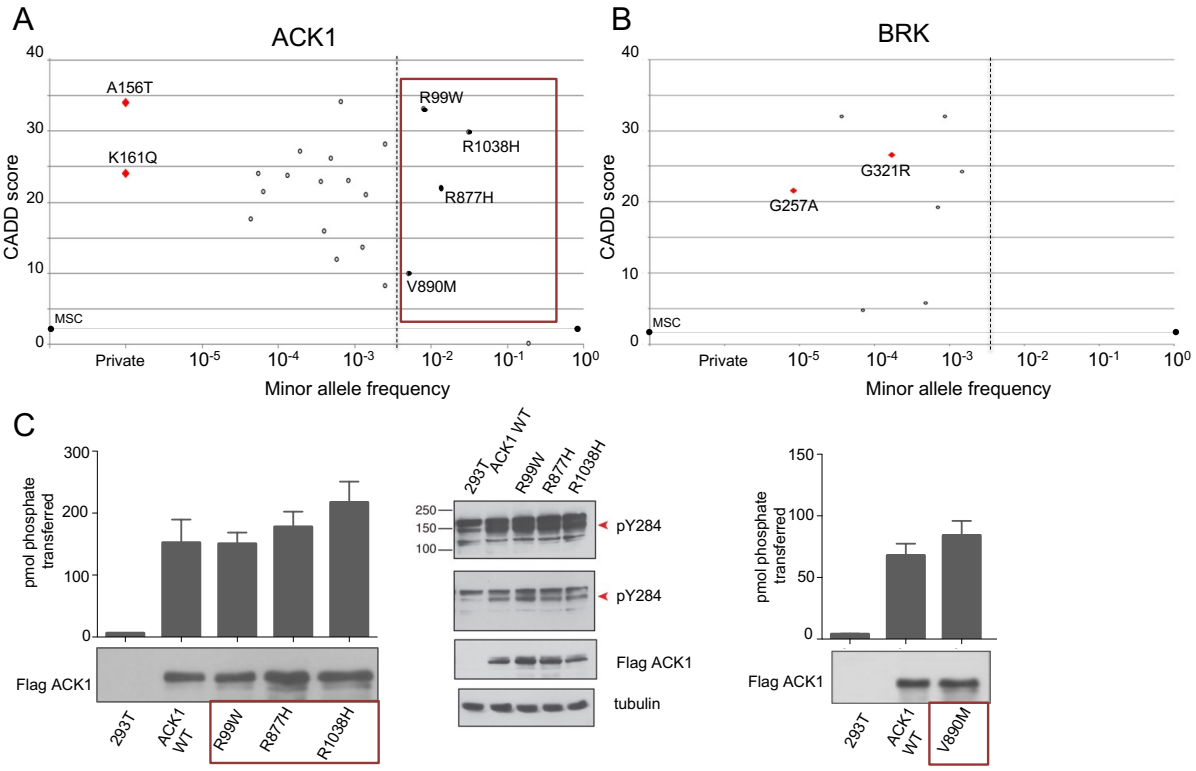

Figure 2-figure supplement 2. Homozygote mutant alleles reported in public database gnomAD with MAF> 0.005 don't affect the kinase activity of ACK1. (A, B) ACK1 and PTK6 homozygous mutants reported in gnomAD database (A) CADD score (*y* axis) plotted against minor allele frequency (MAF, *x* axis) for the mutations found in our patients and homozygous ACK1 missense and LOF variations described in the gnomAD database. The black line corresponds to the mutation significance cutoff (MSC). ACK1^{A156T} and ACK1^{K161Q} missense variations are annotated and shown as red diamonds. Variations with MAF>0.005 (right side dotted line) and CADD/MSC high (>1, above black line) have been tested biochemically and shown as filled black circle. (B) CADD score (*y* axis) plotted against minor allele frequency (MAF, *x* axis) for the mutations found in our patients and homozygous BRK missense and LOF variations described in the gnomAD database. The black line corresponds to MSC. BRK^{G257A} and BRK^{G321R} missense mutants are annotated and shown as red diamonds. (**C**) **ACK1^{R99W}, ACK1^{R877H}, ACK1^{R1038H} and ACK1^{V890M} don't impair ACK1 kinase activity.** Immunoprecipitation kinase assay (*on the le*ft). ACK1 was immunoprecipitated from HEK293T cells expressing Flag-tagged ACK1 (WT and mutants) with anti-Flag Ab. The immunoprecipitated proteins were used in duplicated in vitro for kinase reactions with WASP synthetic peptide. Western blot analysis (*on the right*). Lysates from 293T cells expressing Flag-tagged WT or mutant forms (R99W, R877H and R1038H) of ACK1 were probed with anti-ACK1 Tyr(P)^{284} (PY284), anti-Flag and anti-tubulin antibodies (Ab).

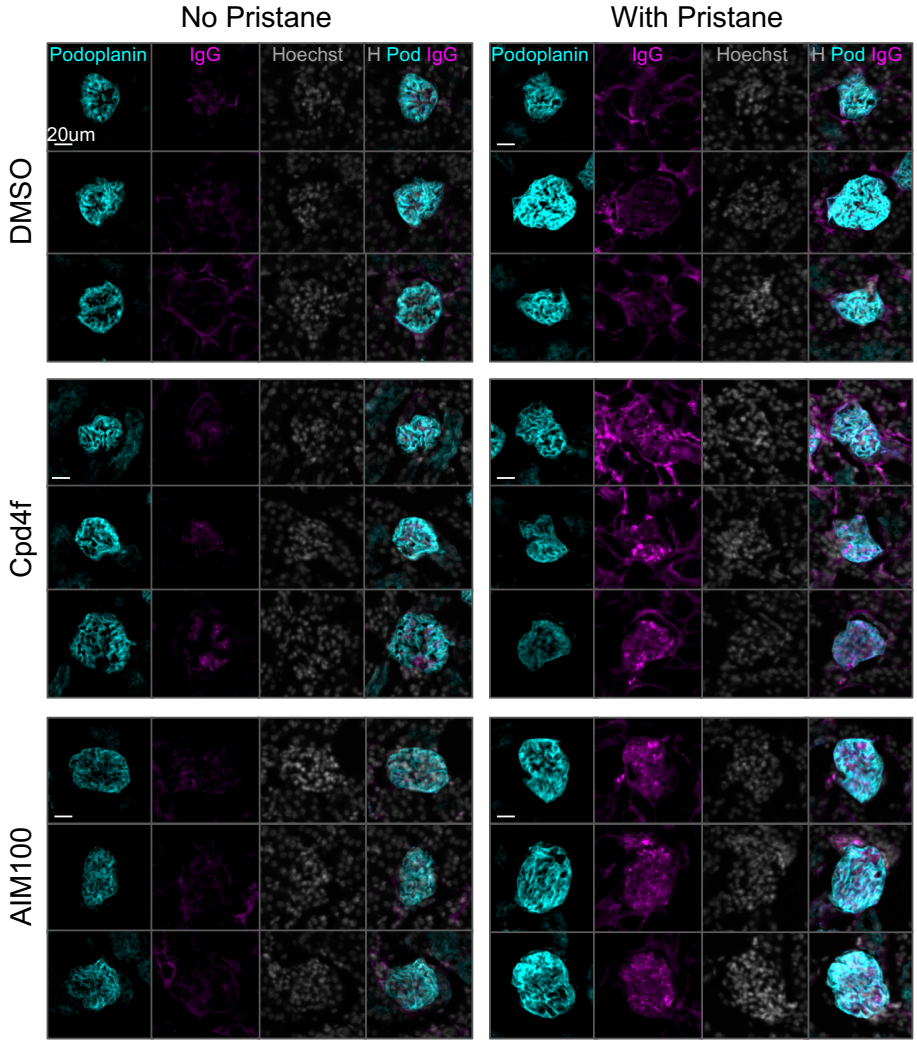

Figure 2-figure supplement 3. Immunofluorescence images for mouse IgG on kidney sections. Representative images of glomeruli displaying the average observed signal on kidney sections from 4 month-old BALB/cByJ female mice which had received weekly intra-peritoneal injection of DMSO (vehicle, 20ul/mice), AIM100 (25mg/kg in 20ul), or Cpd4f (20mg/kg in 20ul/) since the age of five weeks. Kidney sections were stained with Hoechst 33342, anti-mouse IgG, and anti-mouse Podoplanin antibody.

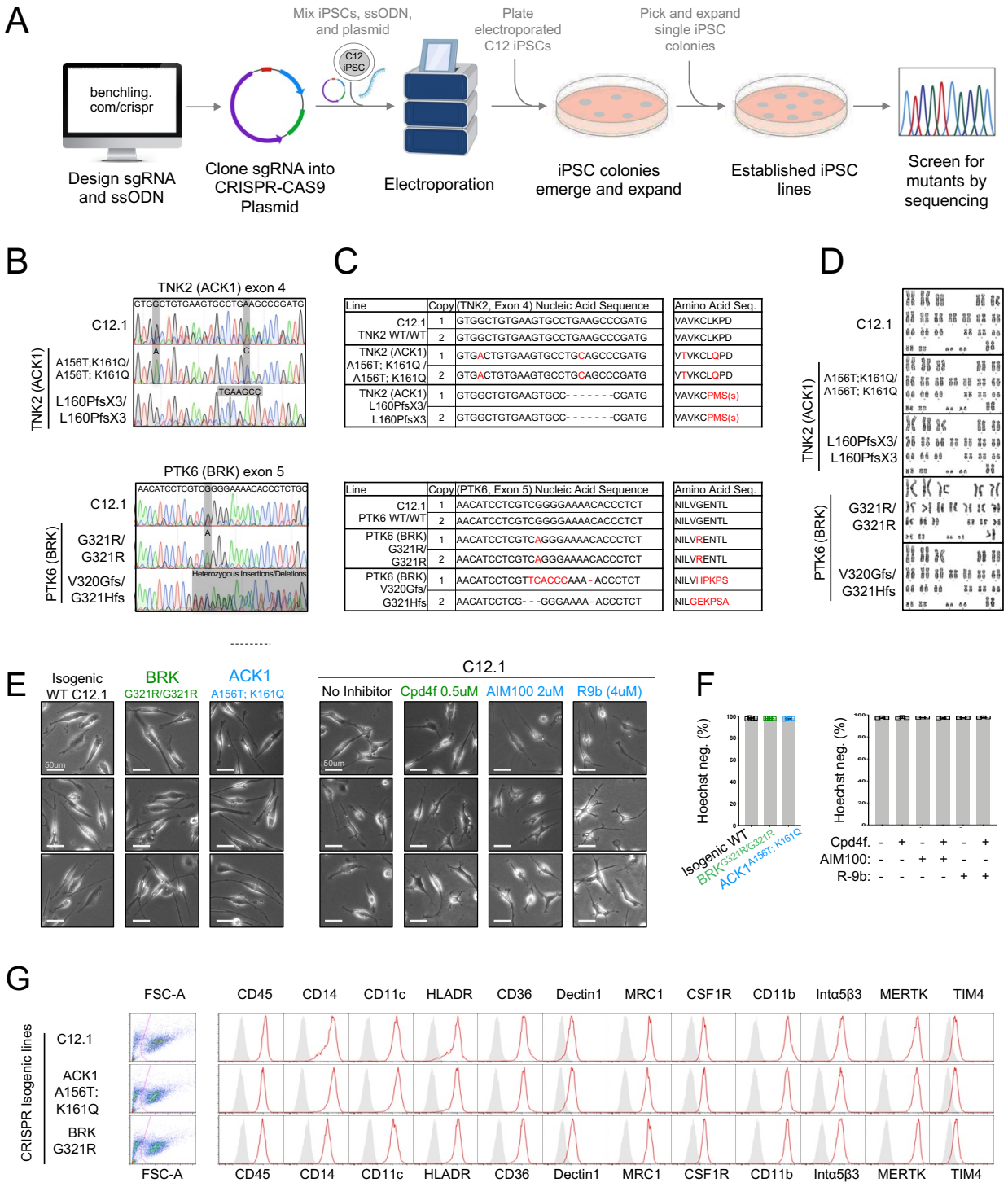

Figure 3-figure supplement 1. Generation and characterization of isogenic control and mutant iPSCs and iPSC-macrophages. (A) Schematic representation of the CRISPR-CAS9 gene editing process to derive C12 isogenic lines with TNK2 or PTK6 mutations. See methods for details. Abbreviations: single guide RNA (sgRNA); Single stranded donor oligonucleotides (ssODN). **(B)** Sanger sequencing of CRISPR-CAS9 modified isogenic iPSC lines. Gray bars indicate position of nucleotide substitutions. **(C)** Nucleic acid and predicted amino acid sequences for both gene copies of TNK2(AKC1) or PTK6(BRK) in CRISPR-CAS9 modified isogenic iPSC lines. Variations from WT are indicated in red. One dash represents one nucleotide deletion. **(D)**

Karyotypes of CRISPR-CAS9 modified isogenic iPSC lines. Chromosome analysis was performed on a minimum of 20 DAPI-banded metaphases. **(E)** Representative brightfield images of Isogenic WT, BRK and ACK1 mutant macrophages (left panel) or WT macrophages treated with designated inhibitors for 2 hours (right panel). Similar morphology observed in n>5 independent experiments. **(F)** Bar plots show percent viability based on Hoechst staining of macrophages derived from isogenic iPSC lines, and percent viability of C12.1 WT macrophages after a 120 min treatment with designated inhibitors. n≥3 replicates per experimental condition. **(G) Flow cytometry** analysis of surface receptor expression on iPSC derived macrophages from isogenic WT and mutant iPSC lines. Histograms show fluorescence intensity for indicated antibodies (red) and FMO controls (grey).

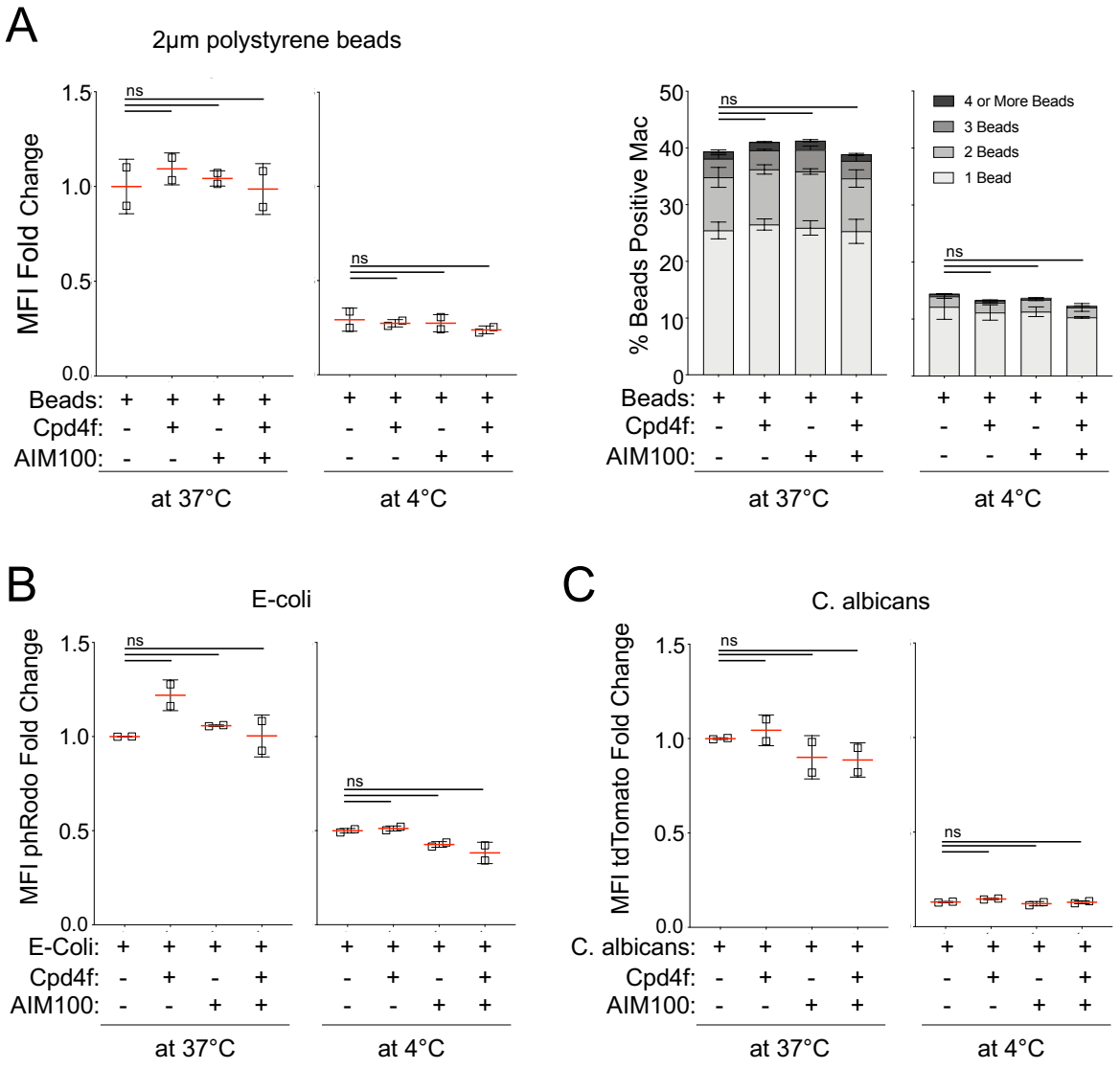

Figure 4-figure supplement 1. ***Engulfment of beads, E. coli, and C. albicans.*** **(A) Phagocytosis of 2µm beads.** iPSC-macrophages (C12 line) pretreated with DMSO, AIM100 (2µM), Cpd4f (0.5µM), or both, were incubated for 60 min at 37C or 4C with red fluorescent 2µm beads. Quantification of uptake is represented as fold change in mean fluorescence intensity (MFI) (670/30 nm) between DMSO treated and inhibitor treated macrophages (left panels). Quantification of uptake as percent red fluorescent (bead) positive macrophages (right panels). n=2 per experimental condition. **(B-C) Phagocytosis of E. coli and C. albicans.** Phagocytosis quantification of pHrodo labeled E. coli (B) or tdTomato fluorescent C. albicans (C) by iPSC-macrophages (C12 line) pretreated with DMSO, AIM100 (2 µM), Cpd4f (0.5 µM), or both, after a 60 min incubation at 37ºC or 4ºC. MFI fold change determined by dividing total MFI (585/15 nm) of individual samples by the average MFI of DMSO treated macrophages. n=2 per experimental condition. P-values in all plots were calculated using an *Anova* test (Tukey's multiple comparisons test).